Journal of Nanomaterials

Applications of Nanobiomaterials in Tissue Repair 2022

Lead Guest Editor: Xiaoming Li
Guest Editors: Hui-Qi Xie, Nicholas Dunne, and Katerina E. Aifantis

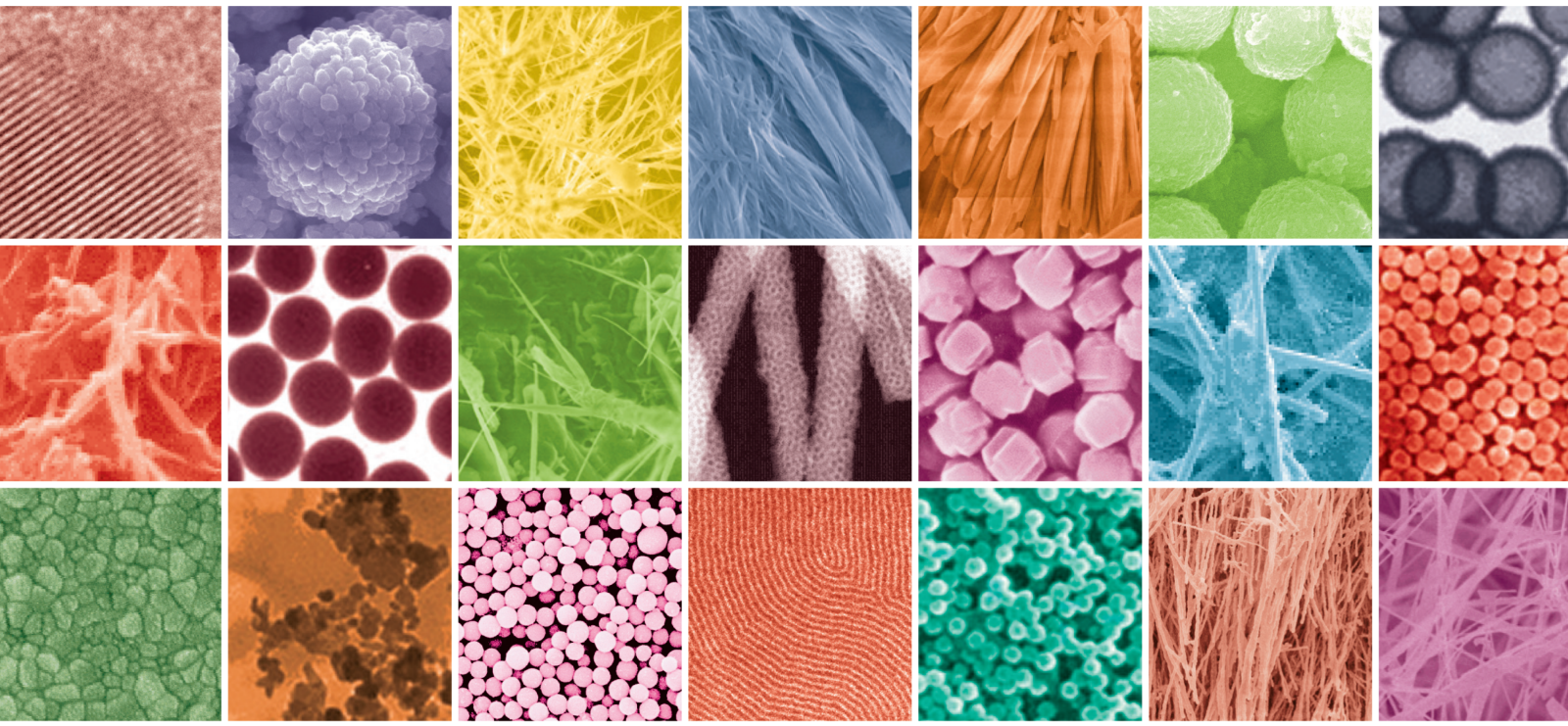

Applications of Nanobiomaterials in Tissue Repair 2022

Journal of Nanomaterials

Applications of Nanobiomaterials in Tissue Repair 2022

Lead Guest Editor: Xiaoming Li
Guest Editors: Hui-Qi Xie, Nicholas Dunne, and Katerina E. Aifantis

Contents

Hindawi
Journal of Nanomaterials
Volume 2022, Article ID 3530620, 13 pages
https://doi.org/10.1155/2022/3530620

Research Article

Establishment of FK506-Enriched PLGA Nanomaterial Neural Conduit Produced by Electrospinning for the Repair of Long-Distance Peripheral Nerve Injury

Ting-Min Xu,[1,2,3] Hong-Yu Chu,[4] Ming Li,[5,6,7] Zuliyaer Talifu,[1,2,3] Han Ke,[1,2,3] Yun-Zhu Pan,[1,2,3] Xin Xu,[1,2,3] Yan-hua Wang,[6,7,8] Wei Guo,[5,6,7] Chuan-Lin Wang,[5,6,7] Feng Gao,[1,2,3] and Jian-Jun Li[1,2,3]

[1]*School of Rehabilitation Medicine, Capital Medical University, Beijing 100068, China*
[2]*Department of Spinal and Neural Function Reconstruction, Beijing Bo'ai Hospital, Rehabilitation Research Center, Beijing 100068, China*
[3]*Beijing Key Laboratory of Neural Injury and Rehabilitation, Beijing 100068, China*
[4]*Department of Comprehensive Rehabilitation, China Rehabilitation Research Center, Beijing 100068, China*
[5]*Trauma Medicine Center, Peking University People 's Hospital, Beijing 100044, China*
[6]*Key Laboratory of Trauma and Neural Regeneration(Peking University, Ministry of Education, Beijing 100044, China*
[7]*National Center for Trauma Medicine, Beijing 100044, China*
[8]*Department of Trauma and Orthopedics, Peking University People 's Hospital, Beijing 100044, China*

Correspondence should be addressed to Feng Gao; gaofeng5960@126.com and Jian-Jun Li; crrclijj@163.com

Ting-Min Xu, Hong-Yu Chu, and Ming Li contributed equally to this work.

Received 24 June 2022; Accepted 28 July 2022; Published 22 August 2022

Academic Editor: Xiaoming Li

Peripheral nerve injury (PNI) is a serious complication of trauma. Autologous nerve transplantation is the gold standard for the treatment of long-distance peripheral nerve defects, but is often limited by insufficient donor sites, postoperative pain, and paresthesia at the donor site. Peripheral nerve tissue engineering has led to the development of neural conduits to replace autologous nerve grafts. This study aimed to evaluate a new type of electrospun nanomaterial neural conduit, enriched with tacrolimus (FK506), which is an FDA-approved immunosuppressant, for the repair of long-distance peripheral nerve injuries. Poly (lactic-co-glycolic acid) (PLGA) nanofibrous films, with FK506, were prepared by electrostatic spinning and rolled into hollow cylindrical nerve vessels with an inner diameter of 1 mm and length of 15 mm. Material characterization, mechanical testing, degradation, drug release, cytotoxicity, cell proliferation, and migration assays were performed in vitro. Long-distance sciatic nerve injuries in rats were repaired in vivo using electrospun nerve conduit bridging, and nerve regeneration and muscle and motor function recovery were evaluated by gait analysis, electrophysiology, and neuromuscular histology. Compared to PLGA, the PLGA/FK506 nanomaterial neural conduit showed little change in morphology, mechanical properties, and chemical structure. In vitro, PLGA/FK506 showed lower cytotoxicity and better biocompatibility and effectively promoted the proliferation, adhesion, and migration of Schwann cells. In vivo, PLGA/FK506 had a better effect on sciatic nerve index, compound muscle action potential intensity and delay time, and nerve regeneration quality 12 weeks post-transplantation, effectively promoting long-distance defect sciatic nerve regeneration and functional recovery in rats. FK506-enriched PLGA nanomaterial neural conduits offer an effective method for repairing long-distance peripheral nerve injury and have potential clinical applications.

1. Introduction

Peripheral nerve injury (PNI) is clinically common and results in loss of motor and/or sensory function, which has a serious effect on the prognosis and quality of life of patients [1–3]. Autologous nerve transplantation has many problems, including limited sources, functional destruction of nerve donor sites, and many clinical complications, whereas allogeneic nerve transplantation has inevitable immune rejection problems [4]. In recent years, tissue engineering nerve conduits with properties beyond autologous nerve grafts have become a potential alternative for repair after PNI [5, 6].

The preparation of neural conduits with excellent performance requires comprehensive consideration of the morphological design, material selection, manufacturing technology, and parameter fine-tuning of the experimental scheme of the conduits to simulate the pipeline microenvironment of nerve regeneration to the greatest extent and promote rapid regeneration and functional control of peripheral nerves [7–9]. Nano-micro scaffolds, made by electrostatic spinning technology, have high specific surface area and porosity, which can better simulate the mechanism of the extracellular matrix and provide a good microenvironment for the effective release of neurotrophins and the rapid growth of nerve cells [10, 11]. The effectiveness of rolling obtained nerve membranes into hollow, multilayer, tubular, and artificial nerve conduits for PNI has been proven in various studies [12, 13].

Poly (lactic-co-glycolic acid) (PLGA), as a common wound suture material certified by the FDA [14–16] and a common tissue engineering material, has been widely used in clinical practice, with great advantages in its mechanical properties and degradation performance. Its proper flexibility, stiffness, and good biocompatibility are conducive to the migration of Schwann cells and endothelial cells [17, 18]. PLGA nanofibers, prepared using electrostatic spinning technology, are an ideal material for the construction of neural conduit scaffolds.

The repair of PNI is inseparable from excellent microsurgical techniques. Currently, epineurium sutures are the main PNI repair technology used clinically, but they have many problems, such as generation of neuromas, nerve misconnection, and mismatch. The resultant effect of nerve repair is far less than expected [1]. Through a series of studies, Jiang Baoguo et al. found that artificial nerve conduits can help guide the axons of peripheral nerves to achieve axial growth. Meanwhile, accurate nerve docking was achieved using the selective regeneration characteristics of peripheral nerves, which effectively reduced the growth of neuromas and the occurrence of long-term peripheral neuralgia and became a successful alternative to traditional peripheral nerve epineurium suturing [19, 20]. Previous research found that in PNI, the broken blood-nerve barrier and axonal exposure to the body fluid environment caused increased local exudation and inflammatory reactions, aggravating secondary injury, degeneration, and necrosis of the nerve, causing neuropathic pain, further affecting the quality of nerve regeneration and repair [21]. Therefore, the inhibition of an overactive immune response at the nerve injury site is essential for the repair of that injury. Tacrolimus (FK506), an FDA-approved immunosuppressant, has been shown to enhance peripheral nerve regeneration. Furthermore, Davis et al. found in his study that multifunctional FK506 embedded, micropatterned PLGA films have potential to be used in the construction of peripheral nerve repair devices [22]. Also, FK506-enriched nanoneural conduits developed by electrospinning technology have been proven to effectively reduce neuroimmune response and promote nerve regeneration [23].

This study aimed to evaluate a new type of nanomaterial neural conduit, enriched with FK506, for the repair of long-distance peripheral nerve injuries.

2. Materials and Methods

2.1. Preparation and Characterization of Electrospinning PLGA Nanofiber Membranes and FK506-Enriched Neural Conduits. 1 g of PLGA (purchased from Jinan Dagang Co., Ltd., Jinan, China) particles was dissolved in 10 mL of mixed solvent (7 : 3, v/v) with trichloromethane (purchased from McLean Reagent Co., Ltd., Beijing, China) and N, N-dimethylformamide (purchased from McLean Reagent Co., Ltd., Beijing, China) and stirred at room temperature for 5 h until the PLGA dissolved completely; it was then prepared as a 10% electrospinning solution.

FK506 (purchased from Selleck, Shanghai, China) was predissolved in dimethyl sulfoxide (DMSO), and a solution with a concentration of 40 μg/mL was prepared. Then, 1 mL of the FK506 solution was added to the electrospinning solution and stirred for 5 h (500 RPM). This solution was loaded into a 20-mL syringe, and the spinning voltage of the electrospinning machine was set at 20 kV, the flow rate of the solution was set at 0.5 mL/h, the distance of the receiving device was set at 16 cm, the temperature was set at 25°C, and the humidity was set at 40%. FK506-enriched PLGA nanofiber membranes, with a thickness of 0.1 mm, were obtained. The membranes were cut into small pieces, prepared, and rolled by a steel needle into a hollow cylindrical nerve conduit with an inner diameter of 1 mm and a length of 15 mm.

2.1.1. Morphology Testing of the Nanofiber Membrane. The nanofibers were cut into appropriate sizes and gold-sprayed for 60 seconds. The morphologic characteristics of the nanofibers were examined using scanning electron microscopy (SEM). In addition, the diameter distribution of the nanofibers in the SEM images was analyzed using ImageJ software.

2.1.2. Fourier Transform Infrared Spectrometry. PLGA and PLGA/FK506 nanofibers were tested in the range of 4000-600 cm^{-1} using ATR-FTIR to analyze the chemical structure of the nanofibers.

2.1.3. Mechanical Properties Measurement. The nanofibers were cut into 50 mm × 20 mm pieces. The thickness of each sample was measured using a spiral micrometer, and the mechanical properties of the nanofibers were tested with a tensile tester. The tensile speed used was 10 mm/min.

The other organic reagents used in this part of the study were purchased from Sinopharm (Beijing, China). Other biological reagents were purchased from Sangong Bioengineering Co., Ltd. (Shanghai, China). The equipment used included a field emission SEM (Hitachi SU8010, Japan), an energy scattering spectrometer (EDS, IXRF SDD3030), Fourier transform infrared spectrometer (FTIR, Thermo Scientific, Nicolet 6700, USA), a tension tester (MarK-10, ESM303 motorized tension/compression test stand, USA), and a confocal laser microscope (Olympus FV1000, Japan).

2.2. Performance Evaluation of In Vitro Degradation and Drug Release of the Nerve Conduits. A certain mass of PLGA and PLGA/FK506 nanofiber membranes was weighed, and the initial mass of the sample was recorded as M_0. The samples were placed into a 10-mL phosphate buffered saline (PBS) solution and oscillated in a shaker at 37°C and 100 RPM. The scaffolds were removed in the first, second, third, fourth, and fifth weeks. The samples were washed with deionized water, freeze-dried, and weighed, and the mass after degradation was recorded as M_1. The degradation efficiency was calculated according to the following formula:

$$\text{Degradation Efficiency}(\%) = \frac{M0 - M1}{M0} \times 100\%. \quad (1)$$

Each group of samples was tested three times and the results were averaged.

The release behavior of FK506 from PLGA/FK506 nanofibers was measured. First, the FK506 DMSO solution was diluted with PBS into standard solutions of 140, 120, 100, 80, 60, 40, and 20 μg/mL. The FK506 solution of each concentration was placed in a 96-well plate, and the standard curve was measured three times for each concentration. The 60 mg nanofiber membrane was immersed in a 3-mL PBS solution (7.2-7.4), and all the released solution was taken out at certain time points. The released amount was determined using a UV spectrophotometer (HV-VIS, Hitachi U-4100), and 3 mL fresh PBS solution was added for the next test.

2.3. Evaluation of the Safety and Effectiveness of the Nerve Conduits in In Vitro Cell Experiments. Good biocompatibility is an important index for the evaluating neural conduits. In this study, the MTT (3-(4,5-dimethylthiazol-2-yl)-2,5-diphenyltetrazolium bromide) assay and cell viability staining were used to evaluate the biocompatibility of the materials. Mouse embryonic fibroblast (NIH/3T3) cells were purchased from the National Infrastructure of Cell Line Resource (Beijing, China) and cultured in Dulbecco's modified eagle medium (DMEM) high glucose (Gibco, Carlsbad, CA, USA) with added 10% fetal bovine serum (Gibco) and 1% penicillin-streptomycin (Gibco). The cell suspension was diluted to 1×10^4/mL. Cell suspensions (100 μL) were added to each well of the 96-well plates, and the nanofiber nerve conduit samples were then added to obtain concentrations of 5000, 2500, 1250, 625, 312.5, and 156.25 μg/mL. Five parallel experiments were conducted for each group of cells, and the materials and cells were co-cultured for 24 h. Thereafter, 10 mL MTT reagent was added to each well, and the culture was continued for 4 h. Then, the cell culture plate was removed, the supernatant was removed, and 100 μL DMSO solution was added to each well. The optical density (OD) values of the cells were measured using an enzyme standard instrument (SpectraMaxM2, Molecular Devices, Sunnyvale, CA, USA).

To further evaluate the effectiveness and safety of the neural conduits, the proliferation, adhesion, and migration of Schwann cells on the conduits were observed. Rat Schwann cells (ATCC CRL-2765, rat Schwann cell lines) were purchased from the cell bank of the Chinese Academy of Sciences (Shanghai, China) and cultured in DMEM high glucose (Gibco, Carlsbad, CA, USA) supplemented with 10% fetal bovine serum (Gibco) and 1% penicillin-streptomycin (Gibco). The nanofiber material was sterilized for 1 h, and the PBS buffer was fully watered and washed three times. The residual ethanol was removed, and the scaffold was immersed in a completely prepared medium for later use. Schwann cells in culture vials were then digested with trypsin, diluted to a concentration of 10^4 cells per well, and inoculated into the nanofiber membranes.

On the second day after cell seeding, the morphology of the Schwann cells on the nanofibers was examined by SEM (HITACHI SU8010, Japan) to observe the cell adhesion. The samples were cleaned with PBS and treated with UV sterilization. Schwann cells were spread on the nanofiber membrane, fixed with 4% paraformaldehyde for 1 h. The paraformaldehyde was then removed, and the cells were washed twice with PBS. Gradient dehydration was performed with ethanol solutions of different concentrations (30%, 50%, 70%, 80%, 90%, and 100%), with each concentration gradient used for 10 min. The samples were dried at room temperature, sprayed with gold, and viewed using SEM.

Schwann cells were observed and compared on the first, second, and third days by the cell scratch (repair) method. Schwann cells were laid flat on the nanofiber membrane and cross-scratched on the surface with a spearhead. The cells were washed with PBS three times to remove the scratched cells and then added to the medium and cultured in an incubator. Photographs of the samples were obtained at 24 h, 48 h, and 72 h.

2.4. Evaluation of the Safety and Effectiveness of the Nerve Conduits In Vivo in Rats

2.4.1. Experimental Animals and Grouping. Thirty 8-week-old female Sprague-Dawley rats, weighing 200-220 g, were provided by Weitonglihua Experimental Technology Co., Ltd. The rats were randomly divided into three groups of 10 rats each: the PLGA, PLGA/FK506, and autologous nerve transplantation groups.

2.4.2. Surgical Methods and Procedures. Inhalation anesthesia with 3% isoflurane (RWD Life Science, Shenzhen, China) was administered. After anesthesia, the rats were fixed on the operating table in a prone position. After skin disinfection of the right hind limb, the skin and subcutaneous tissues were cut

layer by layer, and the muscle space was bluntly separated to fully expose the sciatic nerve. The sciatic nerve was cut to 15 mm under a surgical microscope. In the PLGA and PLGA/FK506 groups, the two ends of the sciatic nerve were inserted for 1 mm into each end of the nerve conduit and fixed with an 8/0 medical suture. In the autologous nerve transplantation group, the 15-mm sciatic nerve was rotated 180° and then resutured to the two nerve ends with an 8/0 medical suture. The surgical site was douched with normal saline, the muscle and skin were sutured layer by layer with 4/0 medical sutures, and the skin incision was disinfected with iodophor. The rats were closely monitored for infection after the operation.

2.4.3. Gait Analysis. The gait of each group was recorded and analyzed using a CatWalk XT animal gait analyzer (Noldus, Wageningen, The Netherlands) after 12 weeks. The rats were trained for adaptability in advance, and the formal experiment began after the rats could walk continuously on the track. After the experiment, the normal side footprint length (NPL), the operative side footprint length (EPL), the normal side toe width (NTS), the operative side toe width (ETS), the normal side middle toe distance (NIT), and the operative side middle toe distance (EIT) were measured. The sciatic nerve function index (SFI) was calculated according to the following formula: $\mathrm{SFI} = 109.5\,(\mathrm{ETS} - \mathrm{NTS})/\mathrm{NTS} - 38.3\,(\mathrm{EPL} - \mathrm{NPL})/\mathrm{NPL} + 13.3(\mathrm{EIT} - \mathrm{NIT})/\mathrm{NIT} - 8.8$.

2.4.4. Electrophysiological Examination. After the gait analysis, the rats were anesthetized with a 3% isoflurane inhalation. The rats were fixed in a supine position on the operating table, and the right sciatic nerve and gastrocnemius muscle were exposed. Connective tissue surrounding the sciatic nerve was thoroughly removed under the surgical microscope. The recorded electrodes were inserted into the gastrocnemius muscle, and stimulation electrodes were successively placed at the proximal and distal sciatic nerve anastomosis. The amplitude and latency of the compound muscle action potential (CMAP) were recorded using a Synergy Electrophysiology Instrument (Oxford, UK).

2.4.5. Materials and Fixation. After electrophysiological examination, the regenerated sciatic nerve and gastrocnemius muscle of the rats were completely removed under deep anesthesia, and the rats were euthanized with carbon dioxide. The gastrocnemius muscle was immersed in 4% tissue cell fixative and preserved at 4°C for subsequent Masson staining. The sciatic nerve was immersed in 4% tissue cell fixative and preserved at 4°C for subsequent immunostaining.

2.4.6. Muscle Masson Staining. Muscle specimens were removed from the 4% tissue cell fixative solution. Dehydrated, waxed, and embedded, cross-sections were set to 5-μm section thickness. The sections were collected using antistripping slides. Sections were routinely dewaxed to water and Masson stained. After staining, the samples were dehydrated using anhydrous ethanol, made transparent with xylene, and sealed with neutral gum. Muscle fiber morphology was observed under a Leica DM4B microscope, and the cross-sectional area of the muscle fibers in each group was analyzed using the Image-Pro Plus software.

2.4.7. Neuroimmunology Fluorescence Staining. The nerve specimens were removed from the 4% tissue cell fixative solution (Solarbio), dehydrated, embedded in optimal cutting temperature compound (OCT), and sectionalized in cross-section. The frozen section thickness was set to 12 μm, and the sections were collected on slides. After PBS poaching, it was permeated with 0.5% Triton-X100 and blockaded in 5% bovine serum albumin (BSA). The primary antibodies used were rabbit anti-S100 (1 : 200; Sigma-Aldrich) and mouse anti-NF200 (1 : 200; Sigma-Aldrich). After incubation at 4°C overnight, secondary antibodies were Alexa Fluor 594 antirabbit IgG (1 : 200, ZSGB-BIO) and Alexa Fluor 488 antimouse IgG (1 : 200, ZSGB-Bio). The nuclei were stained with 4',6-diamidino-2-phenylindole (DAPI).

2.5. Statistical Analysis. SPSS 26.0 software (IBM Corp., NY, USA) was used for statistical analysis, and $\bar{x}\pm s$ was used to represent quantitative data. The one-way analysis of variance (ANOVA) was used for comparisons between groups. $P < 0.05$ indicated statistical difference, and $P < 0.01$ indicated significant statistical difference.

2.6. Ethics Approval. This study was approved by the Ethics Review Board of the Peking University People's Hospital (2019PHE038) on November 11, 2019, and followed the relevant guidelines.

3. Results

3.1. Physical and Chemical Properties of Enriched FK506 Electrospinning PLGA Nanofiber Membranes and Nerve Conduits. In this study, PLGA and PLGA/FK506 nanofiber membranes were prepared by electrostatic spinning technology, and neural conduits were prepared accordingly (process shown in Figures 1(a)–1(c)). SEM shows that the two nanofiber membranes were uniform and flat, with good nanofiber morphology, as shown in Figures 1(c) and 1(f). The average diameter of the PLGA nanofibers was 0.67 ± 0.16 μm (Figure 1(d)), and that of the PLGA/FK506 nanofibers was 0.68 ± 0.18 μm (Figure 1(g)). This slight increase may have been due to the addition of FK506.

Figure 1(h) shows the stress-strain curves of the PLGA and PLGA/FK506 nanofibers. A mechanical test can reflect the motor mechanical properties of the nanofibers and imitate the changes in the nerve conduits with the movement of the rat when walking. The tensile test results show that the mechanical strength of the nanofibers decreased slightly after the addition of FK506.

FTIR characterization further confirmed the chemical structure of the nanofibers (Figure 1(i)). As shown in Figure 1(d), the characteristic absorption peaks of the PLGA nanofibers are between 1758 cm^{-1} and 1455 cm^{-1} due to the C=O and -CH_2 stretching vibrations. The characteristic absorption peak at 1387 cm^{-1} was due to the stretching vibration of -CH_3. The characteristic absorption peaks at 1183 cm^{-1} and 1083 cm^{-1} were due to the asymmetric stretching vibration of C-O-C in the ester group. PLGA/FK506 had the same characteristic absorption peak as PLGA, indicating that the addition of FK506 did not affect the chemical structure of PLGA.

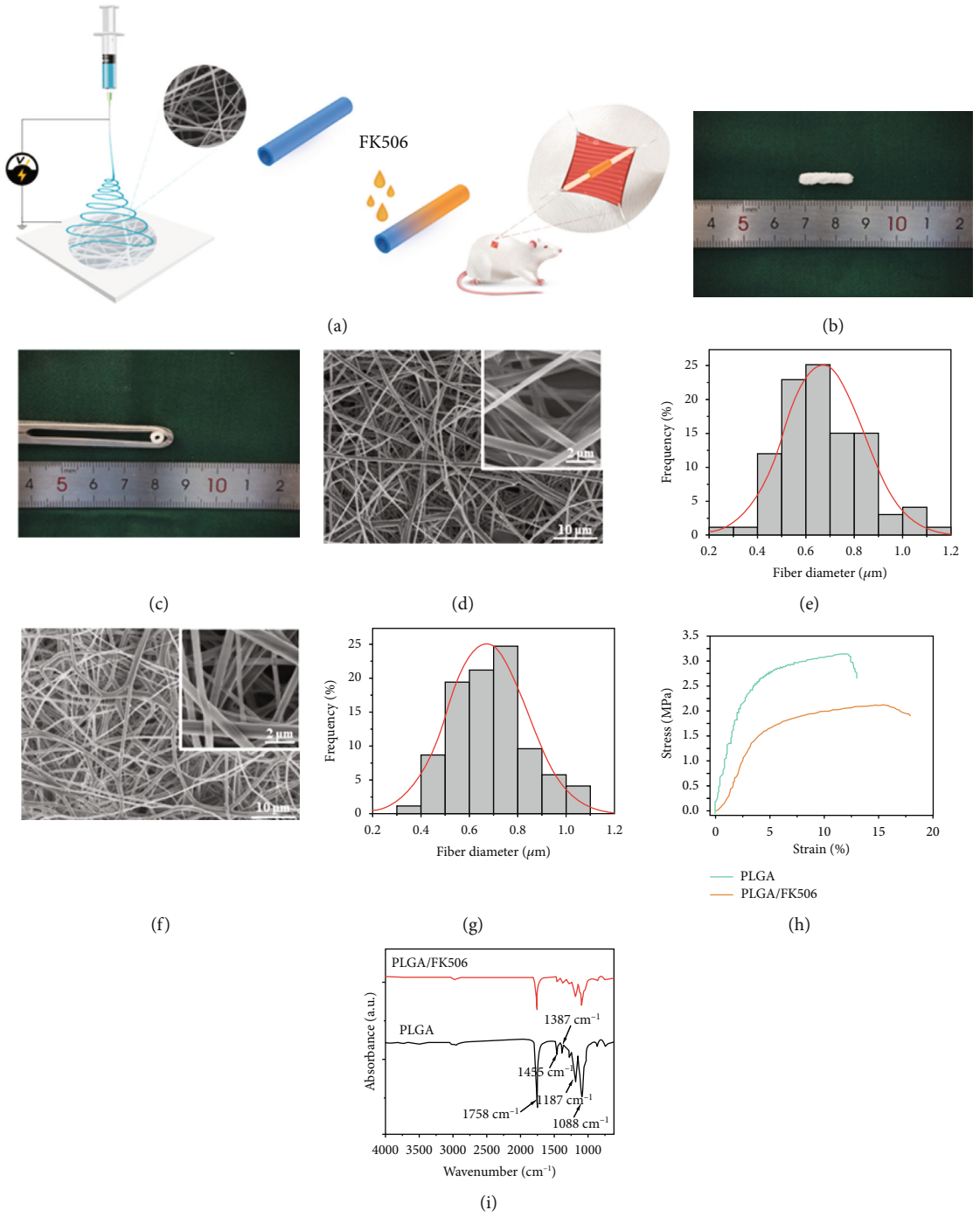

Figure 1: Preparation of nanofiber membranes and nerve conduits. (a) Experimental process. (b and c) Macroscopic views of the conduits. (d and e) SEM morphology and fiber diameter distribution of the PLGA nanofiber membrane ($n = 100$). (f and g) SEM morphology and fiber diameter distribution of the PLGA/FK506 nanofiber membrane ($n = 100$). (h and i) Tensile properties of the nanofibers and the FTIR spectra.

These results indicate that the addition of FK506 had no significant effect on the physical and chemical properties of the PLGA nanofibers and that PLGA retains its good mechanical properties and other advantages.

3.2. Performance Evaluation of In Vitro Degradation and Drug Release of the Nerve Conduits. The weight loss rate and change in material morphology during the degradation process are important characteristics of the material degradation properties. It can be seen from Figure 2(a) that the nanofibers gradually became thicker and that adhesiveness occurred during the degradation process. According to the weight loss rate of the material in Figure 2(b), the degradation of the nanofiber membrane did not change significantly in the first two weeks, but began to gradually degrade from the third week. By the fifth week, the degradation degree

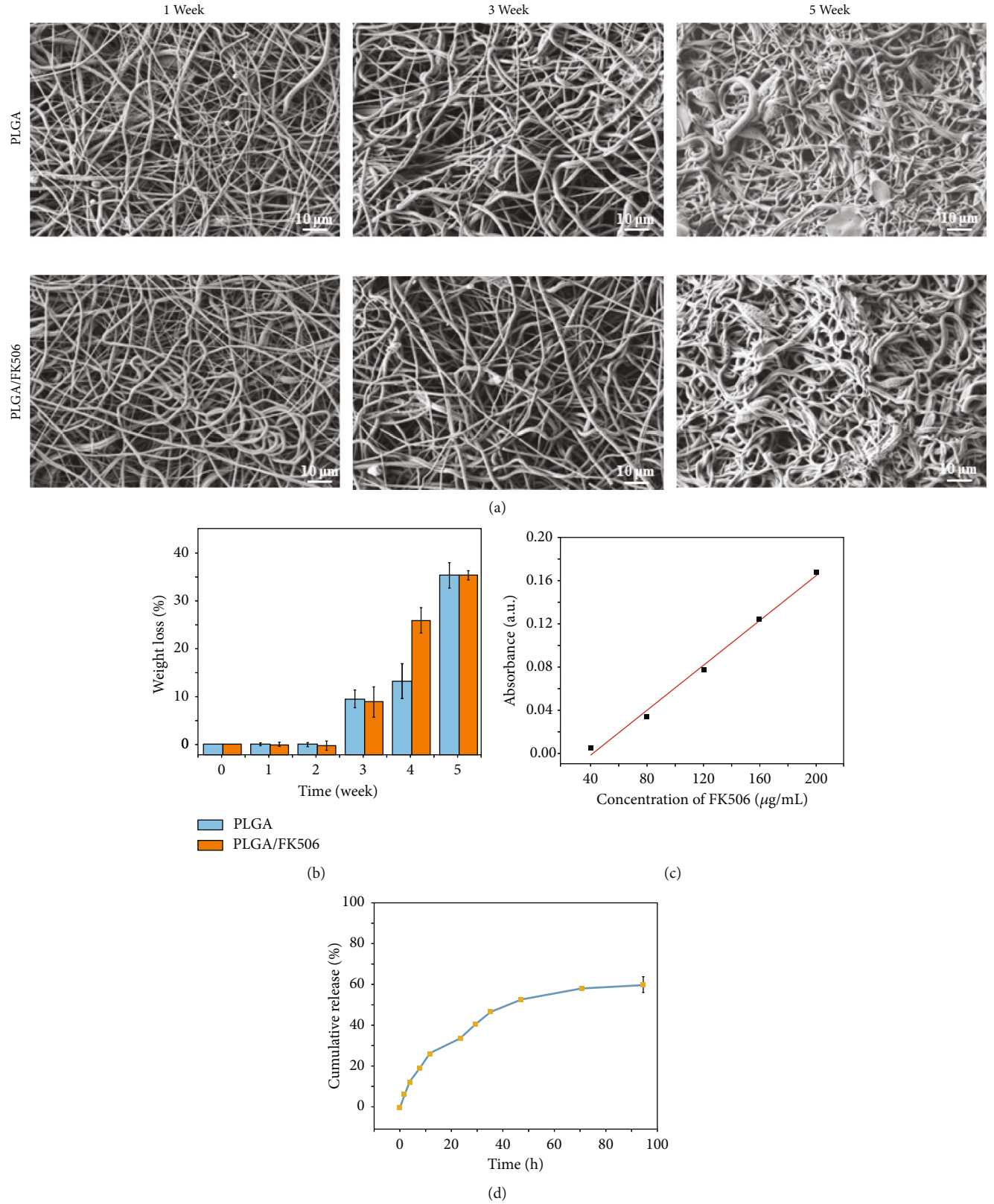

Figure 2: Degradation and release of nanofibers in vitro. (a) SEM diagram of the degradation process of PLGA and PLGA/FK506 nanofibers at the 1 week, 3 weeks, and 5 weeks. (b) Degradation rate of the two nanofibers after 5 weeks. (c) Standard release curves of FK506. (d) Drug release process of the PLGA/FK506 nanofiber membrane.

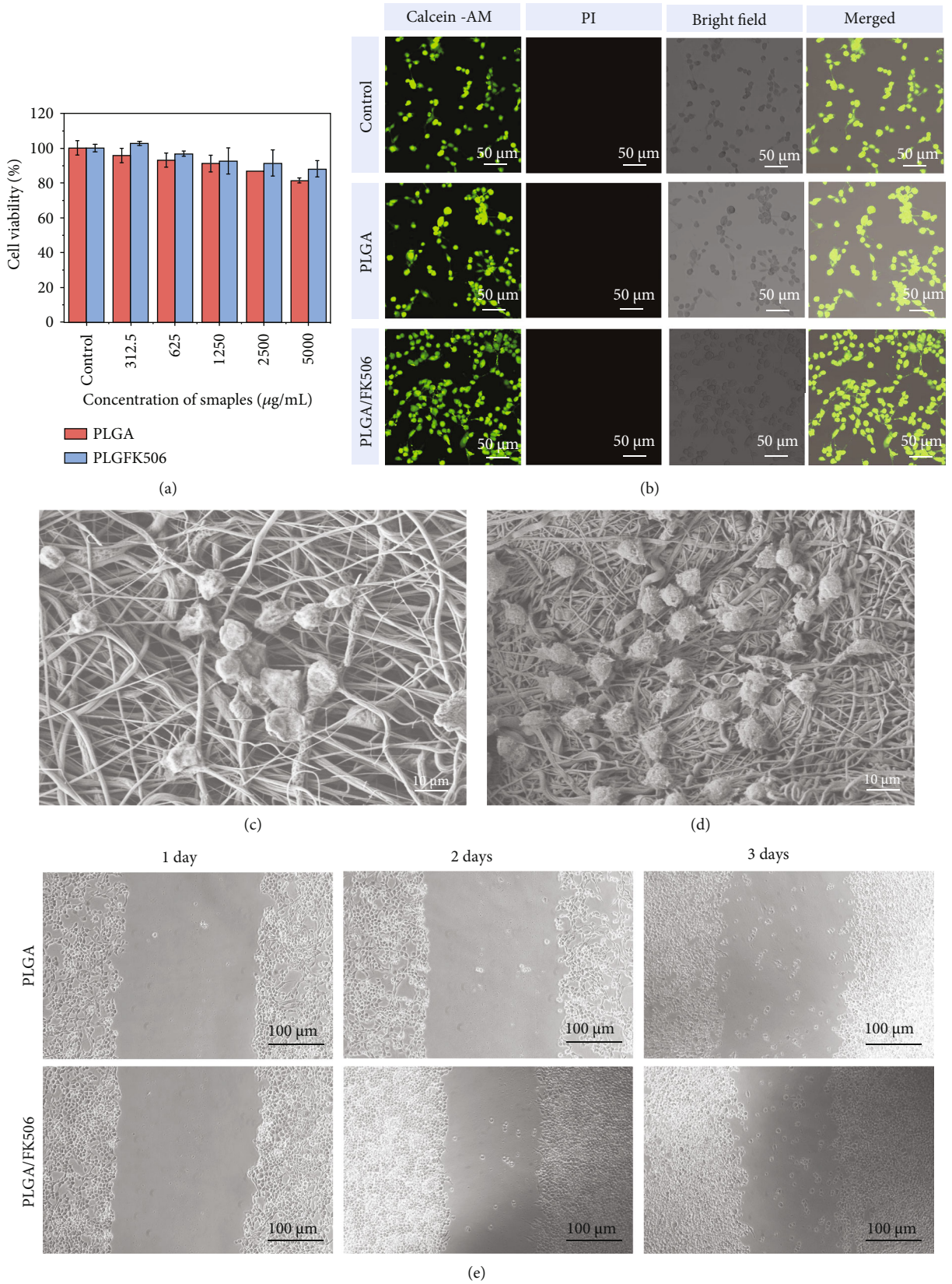

Figure 3: Tests of safety and efficacy of different nanofibers in vitro. (a) Cell activity analysis. (b) Cell viability staining analysis. (c) Cell adhesiveness on PLGA nanofiber membrane. (d) Cell adhesiveness on PLGA/FK506 nanofiber membrane. (e) Cell migration image on different fiber surfaces.

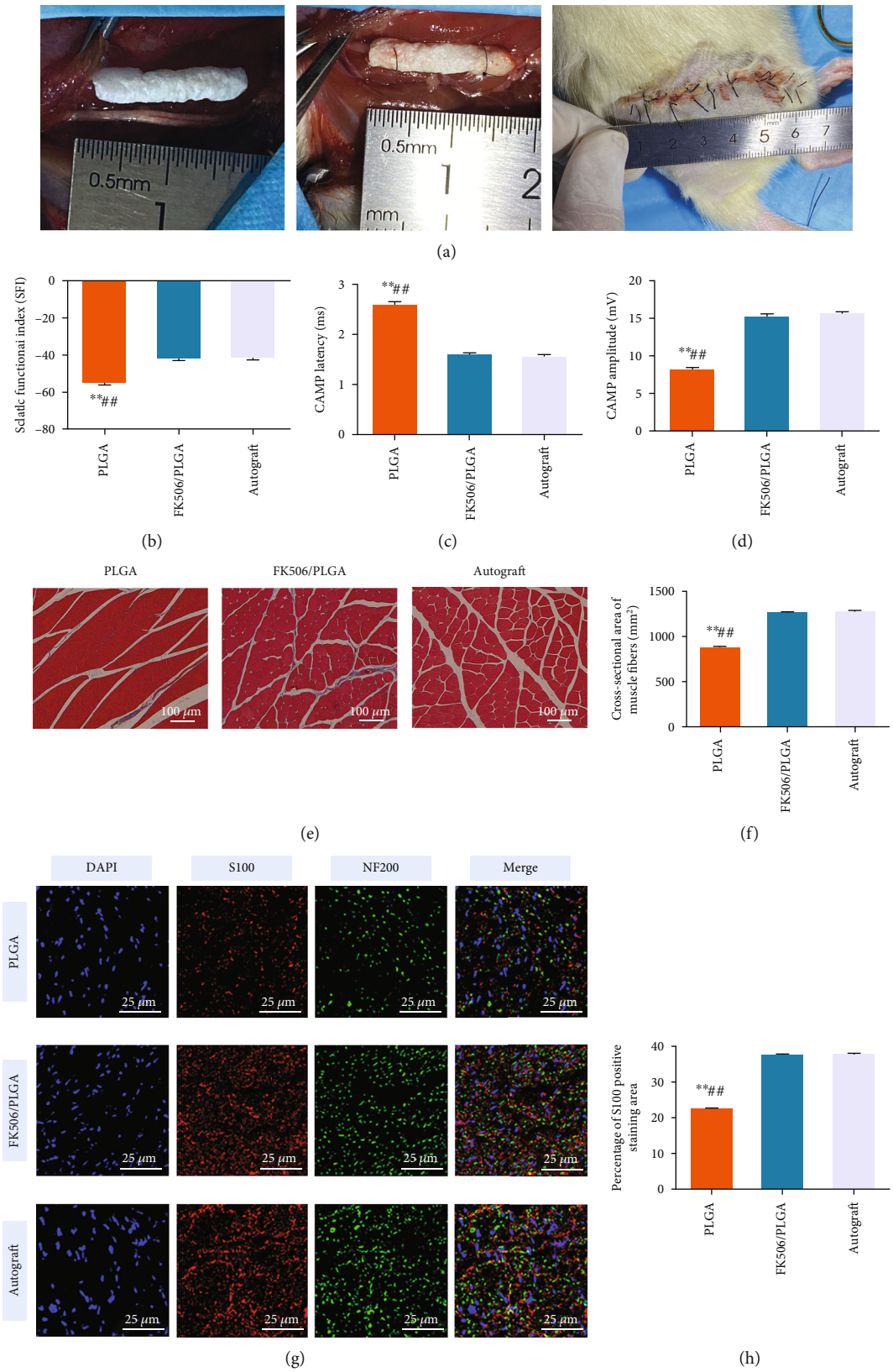

Figure 4: Continued.

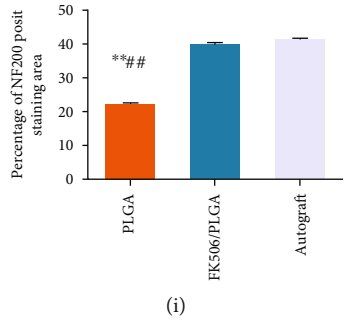

(i)

Figure 4: Comparison of experimental results in vivo in rats. (a) Surgical experiment process on rats. (b) Function index of the sciatic nerve after 12 weeks in each group. (c) Amplitude of the compound muscle action potential after 12 weeks in each group. (d) Incubation period of the compound muscle action potential after 12 weeks in each group. (e) Masson staining diagram of the target muscle (gastrocnemius) after 12 weeks in each group. (f) Statistical diagram of the cross-sectional area of the muscle fiber in each group. (g) Immunofluorescence staining diagram of the nerve. (h) S100 positive area graph. (i) NF200 positive area graph. Note: $n = 10$, **compared with the PLGA/FK506 group, $P < 0.01$; ## compared with the autologous transplantation group, $P < 0.01$.

was 35.2%. These results indicate that the two nanofibers have good degradability and can be used as stable passages for support during nerve repair.

The release control of FK506 is related to the time node and cycle of its action, which ultimately affects the results of nerve repair. The release process of FK506 from the PLGA nanofibers is shown in Figure 2(d). Burst release of FK506 occurred at the beginning of the process. After 12 h the release reached 26.31%, and after 48 h, the release reached 52.98%, and it then gradually stabilized.

3.3. Evaluation of the Safety and Effectiveness of Nerve Conduits in Cell Experiment. The biocompatibility of the materials used for nerve conduits has always been a focus and is an important evaluation index of biomaterials. In this study, MTT analysis and cell viability staining were used to evaluate the biocompatibility of the PLGA/FK506 nanofibers. As shown in Figure 3(a), the survival rate is higher than 80% after the nanofibers and cells of PLGA and PLGA/FK506 were co-cultured. As shown in Figure 3(b), nanofiber-treated cells show green fluorescence according to the cell viability staining analysis, indicating good biocompatibility. Concurrently, to some extent, the above results show that FK506 is beneficial for the proliferation of Schwann cells.

To verify that a PLGA neural scaffold with FK506 could better promote the adhesion of Schwann cells, we conducted the following experiments. Schwann cells grew and spread well on the surface of the PLGA/FK506 nanofibers, and the number of cells on the surface of the PLGA/FK506 nanofibers was higher than that on the surface of the PLGA nanofibers (Figures 3(a) and 3(d)). Meanwhile, the cell migration results (Figure 3(e)) showed that there were far more Schwann cells on the scratch surface of the PLGA/FK506 nanofibers, indicating that FK506 had a better guiding and promoting effect on Schwann cell growth and migration.

These results suggest that the addition of FK506 to PLGA nanofibers reduced cytotoxicity; improved biocompatibility; and promoted the adhesiveness, proliferation, and migration of Schwann cells. PLGA nanofiber with added FK506 is more suitable as a biological material for the constructing neural conduits.

3.4. Evaluation of Safety and Effectiveness of the Nerve Conduits In Vivo in Rats. The evaluation of the PLGA/FK506 nerve conduits, combined with a small sleeve suture technique for sciatic nerve injury repair in rats, has progressed further in Figure 4(a). The performance and repair effects of the prepared nerve conduits were observed for 12 weeks.

The SFI results were obtained by recording and analyzing the gaits of the rats. SFI results closer to zero indicate better functional recovery. As shown in Figure 4(b), the SFI in the PLGA group is lower than that in the PLGA/FK506 and the autologous transplantation groups, and the difference is statistically significant ($P < 0.01$). There was no statistically significant difference in SFI between the PLGA/FK506 and the autologous transplantation group ($P > 0.05$). Currently, CMAP is currently widely used by domestic and foreign scholars as an indicator of the effectiveness of peripheral nerve repair. Its peak amplitude is associated with the number of muscle fibers innervated, while its delay time is associated with the regeneration of the nerve myelin sheath thickness. The CMAP reflects the regeneration of motor nerves in the injured nerve and recovery of target muscle function comprehensively. Figure 4(c) shows that the CMAP delay time in the PLGA group was greater than that in the PLGA/FK506 and the autologous transplantation groups; the difference was statistically significant ($P < 0.01$), whereas there was no significant difference in the CMAP delay time between the PLGA/FK506 and the autologous transplantation groups ($P > 0.05$). Figure 4(d) shows that the amplitude of CMAP in the PLGA group was significantly smaller than that in the PLGA/FK506 and autologous transplantation groups ($P < 0.01$). There was no statistical difference in the CMAP amplitude between the PLGA/FK506 and the autologous transplantation groups ($P > 0.05$). These results indicate that neurological function recovery in the PLGA/FK506 group was close to that of the autologous transplantation group and far better than that in the PLGA group.

As gastrocnemius muscle innervation is dominated by the sciatic nerve, recovery of the gastrocnemius muscle may also indicate recovery of nerve function. As shown in

Figures 4(e) and 4(f), the cross-sectional area of the muscle fiber of the PLGA group is significantly smaller than that of the PLGA/FK506 and the autologous transplantation groups ($P < 0.01$). There was no significant difference between the PLGA/FK506 and autologous transplantation groups ($P > 0.05$). The cross-sectional area of the target muscle fiber can also reflect the state of nerve reinnervation of the target muscle. These results indicated that neurological function recovery in the PLGA/FK506 group was similar to that in the autologous transplantation group and far better than that in the PLGA group.

As showed by immunofluorescence staining in Figure 4(g), Schwann cells are marked by red S100 and neurons by green NF200. As shown in Figures 4(h) and 4(i), the positive area ratios of S100 and NF200 in the PLGA group are both significantly smaller than those in the PLGA/FK506 and autologous transplantation groups ($P < 0.01$). In contrast, there were no significant differences in the S100 and NF200 positive area ratios between the PLGA/FK506 and autologous transplantation groups ($P > 0.05$). These results indicated that the quality of the regenerated nerve in the PLGA/FK506 group was similar to that in the autologous transplantation group and much better than that in the PLGA group.

4. Discussion

Autologous nerve transplantation is the gold standard treatment for repair and regeneration after peripheral nerve injury [24]. The disadvantages of this technique include the limited availability of autologous peripheral nerve tissue for transplantation and donor site morbidity, such as localized anesthetic regions and painful neuroma formation [25]. Therefore, there is a need for new treatments that can replace autologous nerve grafting. Neural conduits have become the best alternative to autologous nerve transplantation for the repair of PNI [26]. Injured nerve regeneration is limited to long-distance nerve defects [27].

After peripheral micro nerve injury, the changes in the local microenvironment of the injured nerve have a significant influence on the repair process and results. Increasing attention has been paid to the establishment of the local microenvironment to improve the repair effect by the exogenous addition of drugs, cellular matrix molecules, or neurotrophic factors, through conduits. The influence of an excessive immune response in the early stage of PNI on the final recovery effect has been brought into prominent focus already [28]. FK506 is a commonly used immunosuppressive drug, and its ability to promote peripheral nerve regeneration is well-established. This is mainly manifested in the following four aspects [29, 30]. First, when FK506 acts on PNI, it can significantly inhibit the expression of IL-6 and the activation of NF-κB in the spinal cord neurons of the injured nerve, which plays an important role in reducing the apoptosis of the injured neurons [31]. Second, FK506 can inhibit fibroblast growth and indirectly promote the proliferation of Schwann cells [29]. Concurrently, FK506 significantly inhibits the local inflammatory response in PNI and reduces the damage caused by the inflammatory response to regenerated axons [29]. Finally, FK506 increases the phosphorylation of GAP-43 through the biological activity of FKBP52 and enhances the activity of growth cones, thereby exerting neurotrophic and neuroprotective effects and promoting the regeneration of neural axons [32]. The effectiveness of FK506 in promoting the regeneration of PNI was also verified in our study. In our study, the PLGA/FK506 group achieves better nerve regeneration results than the PLGA group, as shown in Figure 4, and also confirms the role of FK506 in peripheral nerve repair. In addition, a variety of neurotrophic factors, such as nerve growth factor (NGF), brain-derived neurotrophic factor (BDNF), ciliary neurotrophic factor (CNTF), and vascular endothelial growth factor (VEGF), are beneficial for nerve repair, but their use is limited by the instability and short half-life of nerve factors [33, 34]. To this end, short peptides with cellular properties have been used to simulate the function of nutritional factors, and peptides are stable at different pH values, temperatures, and other environments. Rao et al. added a modified RGI peptide (Ac-RGIDKRHWNSQGG) and KLT peptide (Ac-KLTWQELYQLKYKGIGG) into the interior of the nerve conduit. BDNF and VEGF were simulated, and good results were achieved in repairing sciatic nerve defects in rats [35]. The repair process of PNI involves precise cooperation and complex interactions between numerous cells and molecules. The optimal drug treatment for nerve injury has not yet been determined yet. Therefore, methods for screening the appropriate combination and ratio of many drugs are also worthy of further research and attention.

In addition to the various factors and drugs that promote nerve repair, a sustained release carrier loaded with the drugs is also crucial for the effectiveness of the drugs. The selection of carrier materials and drug loading methods should be considered when constructing of carriers. Aliphatic polyesters are typical degradable polymers that can be used for nerve repair, also for poly (L-lactic acid) (PLLA), poly (glycolic acid) (PGA), polycaprolactone (PCL), and poly (L-lactic co-glycolic acid) (PLGA). Owing to their good mechanical properties and plasticity in physical and chemical properties, these materials are often used as carriers for constructing neural conduits, either alone or in combination with other materials. Among them, PLGA has been widely used in clinical practice for wound sutures, as certified by the FDA [14–16]. PLGA is a well-known polymer, with properties such as good biocompatibility, well-defined biodegradability, and ease of fabrication and has a wide range of applications in biomedical engineering [35]. The advantage of the PLGA nerve conduit is that it is degradable and does not require a second surgery for removal after nerve regeneration. Studies have shown that PLGA has an optimal degradation time which provides sufficient mechanical support for nerve regeneration without hindering nerve regeneration. Previous studies have also shown that PLGA is a suitable material for a nerve conduits [36]. In this study, the degradation of PLGA electrospun nanofibers in vitro is shown in Figure 2(a), indicating its effective support for peripheral nerve regeneration and its excellent degradability.

The drug loading methods of nerve conduits have also been well-studied, from the direct soaking method to the use of nanofibers from electrostatic spinning uniformly distributing factors or drugs in carriers. Later, other methods were developed, such as modification of the surface groups of the carrier, polypeptide crosslinking, multicoating embedding, and canal packing using different materials. However, this increases the complexity of the conduit preparation process and the production transformation. By constructing a RADA16-I-BMHP1 assembled peptide and PLGA composite nanomaterial scaffold, Nune et al. improved the mechanical properties and degradation rate of solitary RADA16-I-BMHP1 assembled peptide scaffolds and promoted the adhesiveness, proliferation, migration, and neural-related gene expression of Schwann cells [37]. Oh et al. prevented invasion of the nerve tissue and concurrently supported the growth of blood vessels by constructing PLGA neural conduits with different pore sizes in the internal and external walls, facilitating the exchange of nutrients and metabolites [38]. In addition to PLGA, Yun Qian applied 3D printing and layer-by-layer casting to construct a graphene-PCL compound nerve conduit with its surface modified by polydopamine (PDA) and arginylglycylaspartic acid (RGD), and such studies related to sciatic nerve repair in rats have been conducted. It significantly promotes the expression and repair of PNI from multiple perspectives, such as electrical conductivity and drug effect [39].

Electrospun nanofibers have great potential for use as regenerative medical scaffolds owing to their permeability, which is structurally similar to the extracellular matrix [40]. Electrospun nanofibers can be used to guide cell morphology, migration, and differentiation. In this study, electrostatic spinning technology was applied to construct a FK506-enriched PLGA nanofiber neural conduit, which further improved its biocompatibility on the premise that physicochemical properties such as PLGA morphology and surface groups were not affected, and mechanical properties were retained. The release process of FK506 in PLGA electrospun nanofibers is shown in Figure 2, which demonstrates that the burst release of FK506 occurred at the beginning of the process and that the release amount reached 52.98% after 48 h and then gradually stabilized. Concurrently, the in vivo and in vitro experiments verify that the PLGA/FK506 nanofibers had better repair effectiveness in nerve injury and further improved the quality of nerve regeneration and repair, as shown in Figure 3. Good performance, the loaded drug, and drug release of the nerve conduit have a great influence on the quality of regeneration and repair in nerve injury.

This study had some limitations. First, although electrospun PLGA as an artificial material simulates the extracellular membrane, it still requires improvement in many respects; for example, other biomaterials can be combined with the electrospun PLGA neural conduit. Second, although the effectiveness of FK506 in nerve regeneration has been universally recognized by many researchers, its mechanism of action when aligned with electrospun PLGA in promoting nerve repair (such as an anti-inflammatory mechanism) in this experiment needs to be further studied from the perspective of immunology and molecular biology in the future. In addition, the FK506-enriched electrospun PLGA used in this study can be further validated by animal experiments in larger mammals or primates.

5. Conclusion

This study sought to apply electrostatic spinning technology to the preparation of an FK506-enriched nanomaterial conduit and to prove its safety and effectiveness. This new conduit was successfully used to repair long-distance sciatic nerve injury in rats. This study demonstrates an effective way to repair long-distance peripheral nerve injuries with potential clinical applications in the future.

Abbreviations

PNI: Peripheral nerve injury
FK506: Tacrolimus
PLGA: Poly (lactic-co-glycolic acid)
DMSO: Dimethyl sulfoxide
SEM: Scanning electron microscopy
PBS: Phosphate buffered saline
MTT: 3-(4,5-Dimethylthiazol-2-yl)-2,5-diphenyltetrazolium bromide
DMEM: Dulbecco's modified eagle medium
OD: Optical density
NPL: Normal side footprint length
EPL: Operative side footprint length
NTS: Normal side toe width
ETS: Operative side toe width
NIT: Normal side middle toe distance
EIT: Operative side middle toe distance
SFI: Sciatic nerve function index
CMAP: Compound muscle action potential
OCT: Optimal cutting temperature compound
BSA: Bovine serum albumin
DAPI: 4',6-Diamidino-2-phenylindole
NGF: Nerve growth factor
BDNF: Brain-derived neurotrophic factor
CNTF: Ciliary neurotrophic factor
VEGF: Vascular endothelial growth factor
PLLA: Poly (L-lactic acid)
PGA: Poly (glycolic acid)
PCL: Polycaprolactone
PDA: Polydopamine
RGD: Arginylglycylaspartic acid.

Data Availability

The data generated and/or analyzed during the current study are not publicly available for legal/ethical reasons but are available from the corresponding author on reasonable request.

Conflicts of Interest

The authors declare that they have no conflicts of interest.

Authors' Contributions

All authors contributed to the conception, writing, critical review, and revision of the manuscript. Tingmin Xu, Ming Li, and Jianjun Li have contributed to the conceptualization; Ming Li, Hongyu Chu, and Guo Wei have contributed to the methodology; Zuliyaer Talifu and Han Ke have contributed to the software; Tingmin Xu, Yunzhu Pan, and Xu Xin have contributed to the validation; Tingmin Xu and Yanhua Wang have contributed to the formal analysis; Ming Li, Feng Gao, and Jianjun Li have contributed to the investigation; Feng Gao and Jianjun Li have contributed to the resources; Hongyu Chu, Chuanlin Wang, and Feng Gao have contributed to the data curation; Tingmin Xu and Hongyu Chu have contributed to the writing—original draft preparation; Tingmin Xu, Ming Li, and Feng Gao have contributed to the writing—review and editing; Ming Li and Zuliyaer Talifu have contributed to the visualization; Jianjun Li has contributed to the supervision; Tingmin Xu and Feng Gao have contributed to the project administration; Feng Gao and Jianjun Li have contributed to the funding acquisition. Ting-Min Xu, Hong-Yu Chu, and Ming Li contributed equally to this work.

Acknowledgments

The authors thank the members in Beijing Key Laboratory of Neural Injury and Rehabilitation and National Center for Trauma Medicine, China. This work was supported by the National Natural Science Foundation of China [Grant No.31640045], the National Natural Science Foundation of China [Grant No. 81901251], the National Natural Science Foundation of China [Grant No. 82071400], the Beijing Natural Science Foundation [Grant No. 7204323], and the Science Foundation of China Rehabilitation Research Center [Grant No. 2019ZX-Q1].

References

[1] P. X. Zhang, N. Han, Y. H. Kou et al., "Tissue engineering for the repair of peripheral nerve injury," *Neural Regeneration Research*, vol. 14, no. 1, pp. 51–58, 2019.

[2] M. L. Wang, M. Rivlin, J. G. Graham, and P. K. Beredjiklian, "Peripheral nerve injury, scarring, and recovery," *Connective Tissue Research*, vol. 60, no. 1, pp. 3–9, 2019.

[3] M. Modrak, M. A. H. Talukder, K. Gurgenashvili, M. Noble, and J. C. Elfar, "Peripheral nerve injury and myelination: potential therapeutic strategies," *Journal of Neuroscience Research*, vol. 98, no. 5, pp. 780–795, 2020.

[4] G. Hussain, J. Wang, A. Rasul et al., "Current status of therapeutic approaches against peripheral nerve injuries: a detailed story from injury to recovery," *International Journal of Biological Sciences*, vol. 16, no. 1, pp. 116–134, 2020.

[5] S. Vijayavenkataraman, "Nerve guide conduits for peripheral nerve injury repair: a review on design, materials and fabrication methods," *Acta Biomaterialia*, vol. 106, no. 1, pp. 54–69, 2020.

[6] Q. Long, B. Wu, Y. Yang et al., "Nerve guidance conduit promoted peripheral nerve regeneration in rats," *Artificial Organs*, vol. 45, no. 6, pp. 616–624, 2021.

[7] B. Wang, C. F. Lu, Z. Y. Liu et al., "Chitin scaffold combined with autologous small nerve repairs sciatic nerve defects," *Neural Regeneration Research*, vol. 17, no. 5, pp. 1106–1114, 2022.

[8] F. Rao, Z. Yuan, D. Zhang et al., "Small-molecule SB216763-loaded microspheres repair peripheral nerve injury in small gap tubulization," *Frontiers in Neuroscience*, vol. 13, no. 13, p. 489, 2019.

[9] P. Meena, A. Kakkar, M. Kumar et al., "Advances and clinical challenges for translating nerve conduit technology from bench to bed side for peripheral nerve repair," *Cell and Tissue Research*, vol. 383, no. 2, pp. 617–644, 2021.

[10] Y. Yan, R. Yao, J. Zhao et al., "Implantable nerve guidance conduits: material combinations, multi-functional strategies and advanced engineering innovations," *Bioactive Materials*, vol. 11, no. 5, pp. 57–76, 2022.

[11] N. U. Kang, S. J. Lee, and S. J. Gwak, "Fabrication techniques of nerve guidance conduits for nerve regeneration," *Yonsei Medical Journal*, vol. 63, no. 2, pp. 114–123, 2022.

[12] Z. Peixun, H. Na, Y. Kou, Y. Xiaofeng, and B. Jiang, "Peripheral nerve intersectional repair by bi-directional induction and systematic remodelling: biodegradable conduit tubulization from basic research to clinical application," *Artificial cells, nanomedicine, and biotechnology*, vol. 45, no. 8, pp. 1464–1466, 2017.

[13] F. Rao, Z. Yuan, M. Li et al., "Expanded 3D nanofibre sponge scaffolds by gas-foaming technique enhance peripheral nerve regeneration," *Artificial cells, nanomedicine, and biotechnology*, vol. 47, no. 1, pp. 491–500, 2019.

[14] P. Lu, G. Wang, T. Qian et al., "The balanced microenvironment regulated by the degradants of appropriate PLGA scaffolds and chitosan conduit promotes peripheral nerve regeneration," *Materials Today Bio*, vol. 12, no. 16, p. 100158, 2021.

[15] M. Okamoto and B. John, "Synthetic biopolymer nanocomposites for tissue engineering scaffolds," *Progress in Polymer Science*, vol. 38, no. 10-11, pp. 1487–1503, 2013.

[16] T. W. Chung, M. C. Yang, C. C. Tseng et al., "Promoting regeneration of peripheral nerves *in-vivo* using new PCL-NGF/Tirofiban nerve conduits," *Biomaterials*, vol. 32, no. 3, pp. 734–743, 2011.

[17] A. C. Pinho, A. C. Fonseca, A. C. Serra, J. D. Santos, and J. F. Coelho, "Peripheral nerve regeneration: current status and new strategies using polymeric materials," *Advanced Healthcare Materials*, vol. 5, no. 21, pp. 2732–2744, 2016.

[18] Z. I. Foraida, T. Kamaldinov, D. A. Nelson, M. Larsen, and J. Castracane, "Elastin-PLGA hybrid electrospun nanofiber scaffolds for salivary epithelial cell self-organization and polarization," *Acta Biomaterialia*, vol. 62, no. 15, pp. 116–127, 2017.

[19] F. Rao, D. Zhang, T. Fang et al., "Exosomes from human gingiva-derived mesenchymal stem cells combined with biodegradable chitin conduits promote rat sciatic nerve regeneration," *Stem cells international*, vol. 2019, no. 2, Article ID e2546367, p. 12, 2019.

[20] S. Liu, L. Zhou, C. Li et al., "Chitin conduits modified with DNA-peptide coating promote the peripheral nerve regeneration," *Biofabrication*, vol. 14, no. 1, 2022.

[21] F. Fregnan, L. Muratori, A. R. Simões, M. G. Giacobini-Robecchi, and S. Raimondo, "Role of inflammatory cytokines in peripheral nerve injury," *Neural Regeneration Research*, vol. 7, no. 29, pp. 2259–2266, 2012.

[22] B. Davis, S. Wojtalewicz, P. Labroo et al., "Controlled release of FK506 from micropatterned PLGA films: potential for application in peripheral nerve repair," *Neural regeneration research*, vol. 13, no. 7, pp. 1247–1252, 2018.

[23] P. Labroo, D. Hilgart, B. Davis et al., "Drug-delivering nerve conduit improves regeneration in a critical-sized gap," *Biotechnology and Bioengineering*, vol. 116, no. 1, pp. 143–154, 2019.

[24] D. Grinsell and C. P. Keating, "Peripheral Nerve Reconstruction after Injury: A Review of Clinical and Experimental Therapies," *BioMed Research International*, vol. 2014, Article ID 698256, 13 pages, 2014.

[25] F. F. A. Ijpma, J. P. A. Nicolai, and M. F. Meek, "Sural nerve donor-site morbidity," *Annals of Plastic Surgery*, vol. 57, no. 4, pp. 391–395, 2006.

[26] S. Houshyar, A. Bhattacharyya, and R. Shanks, "Peripheral nerve conduit: materials and structures," *ACS Chemical Neuroscience*, vol. 10, no. 8, pp. 3349–3365, 2019.

[27] V. Hasirci, D. Arslantunali, T. Dursun, D. Yucel, and N. Hasirci, "Peripheral nerve conduits: technology update," *Medical Devices (Auckland, NZ)*, vol. 7, pp. 405–424, 2014.

[28] A. Baradaran, H. El-Hawary, J. I. Efanov, and L. Xu, "Peripheral nerve healing: so near and yet so far," *Seminars in Plastic Surgery*, vol. 35, no. 3, pp. 204–210, 2021.

[29] K. J. Zuo, T. M. Saffari, K. Chan, A. Y. Shin, and G. H. Borschel, "Systemic and local FK506 (tacrolimus) and its application in peripheral nerve surgery," *The Journal of Hand Surgery*, vol. 45, no. 8, pp. 759–765, 2020.

[30] K. J. Zuo, G. Shafa, K. Chan et al., "Local FK506 drug delivery enhances nerve regeneration through fresh, unprocessed peripheral nerve allografts," *Experimental Neurology*, vol. 341, p. 113680, 2021.

[31] P. Konofaos and J. K. Terzis, "FK506 and nerve regeneration: past, present, and future," *Journal of Reconstructive Microsurgery*, vol. 29, no. 3, pp. 141–148, 2013.

[32] M. Zuber and J. Donnerer, "Effect of FK506 on neurotransmitter content and expression of GAP-43 in neurotoxin-lesioned peripheral sensory and sympathetic neurons," *Pharmacology*, vol. 66, no. 1, pp. 44–50, 2002.

[33] Z. Liu, S. Ma, S. Duan et al., "Modification of titanium substrates with chimeric peptides comprising antimicrobial and titanium-binding motifs connected by linkers to inhibit biofilm formation," *ACS Applied Materials & Interfaces*, vol. 8, no. 8, pp. 5124–5136, 2016.

[34] J. Valencia-Serna, P. Chevallier, R. B. Kc, G. Laroche, and H. Uludağ, "Fibronectin-modified surfaces for evaluating the influence of cell adhesion on sensitivity of leukemic cells to siRNA nanoparticles," *Nanomedicine (London, England)*, vol. 11, no. 9, pp. 1123–1138, 2016.

[35] F. Rao, Y. Wang, D. Zhang et al., "Aligned chitosan nanofiber hydrogel grafted with peptides mimicking bioactive brain-derived neurotrophic factor and vascular endothelial growth factor repair long-distance sciatic nerve defects in rats," *Theranostics*, vol. 10, no. 4, pp. 1590–1603, 2020.

[36] W. Zhao, J. Li, K. Jin, W. Liu, X. Qiu, and C. Li, "Fabrication of functional PLGA-based electrospun scaffolds and their applications in biomedical engineering," *Materials Science & Engineering. C, Materials for Biological Applications*, vol. 59, pp. 1181–1194, 2016.

[37] M. Nune, U. M. Krishnan, and S. Sethuraman, "PLGA nanofibers blended with designer self-assembling peptides for peripheral neural regeneration," *Materials Science & Engineering. C, Materials for Biological Applications*, vol. 62, pp. 329–337, 2016.

[38] S. H. Oh and J. H. Lee, "Fabrication and characterization of hydrophilized porous PLGA nerve guide conduits by a modified immersion precipitation method," *Journal of Biomedical Materials Research. Part A*, vol. 80, no. 3, pp. 530–538, 2007.

[39] Y. Qian, X. Zhao, Q. Han, W. Chen, H. Li, and W. Yuan, "An integrated multi-layer 3D-fabrication of PDA/RGD coated graphene loaded PCL nanoscaffold for peripheral nerve restoration," *Nature Communications*, vol. 9, no. 1, p. 323, 2018.

[40] L. G. Pozzobon, L. E. Sperling, C. E. Teixeira, T. Malysz, and P. Pranke, "Development of a conduit of PLGA-gelatin aligned nanofibers produced by electrospinning for peripheral nerve regeneration," *Chemico-Biological Interactions*, vol. 348, p. 109621, 2021.

Hindawi
Journal of Nanomaterials
Volume 2022, Article ID 3273077, 10 pages
https://doi.org/10.1155/2022/3273077

Research Article

Magnesium–Magnetic Field Synergy Enhances Mouse Bone Marrow Mesenchymal Stem Cell Differentiation into Osteoblasts Via the MAGT1 Channel

Yifan Wang[1], **Xin Wu**[1], **Wenjing Yang**[2], **Pei Feng**[3], **Wei Tan**[1], **Youwen Deng**[1], **and Cijun Shuai**[2,3]

[1]*Department of Spine Surgery, Third Xiangya Hospital, Central South University, Changsha, 410013 Hunan, China*
[2]*Institute of additive Manufacturing, Jiangxi University of Science and Technology, Nanchang 330013, China*
[3]*State Key Laboratory of High-Performance Complex Manufacturing, College of Mechanical and Electrical Engineering, Central South University, Changsha 410083, China*

Correspondence should be addressed to Youwen Deng; drywdeng@163.com and Cijun Shuai; shuai@csu.edu.cn

Received 28 December 2021; Revised 12 February 2022; Accepted 14 February 2022; Published 3 March 2022

Academic Editor: Xiaoming Li

Magnesium ion (Mg^{2+})-based materials are known to exert osteogenic effects that can be enhanced by the bioelectrical properties of magnetic fields. In this study, we examined the effect of a medium-strength static magnetic field (SMF), combined with a Mg^{2+}-containing medium, on the proliferation and osteogenic differentiation of mouse bone marrow mesenchymal stem cells (BMSCs). Mouse BMSCs were divided into a control group, 7.5 mM Mg^{2+} group, 15 mT SMF group, and 7.5 mM Mg^{2+} plus 15 mT SMF group. Osteoblast proliferation was measured using a Cell Counting Kit-8 assay, whereas osteogenic differentiation was detected using alkaline phosphatase (ALP) staining and western blot analysis, respectively. The number and size of calcium nodules were determined using Alizarin Red staining. Compared with those in the control group, the ALP activity, calcium nodule formation, and osteogenic protein expression were promoted in other groups. In particular, Mg^{2+}-SMF had a significant effect after 7 days of intervention and more effectively promoted BMSC differentiation and proliferation than either Mg^{2+} or the SMF alone, suggesting that Mg^{2+}-SMF synergistically contributed to osteogenic differentiation and cell proliferation. To examine their roles in bone differentiation, the *Magt1* and *Creb1* genes were silenced in BMSCs, and the findings indicated that the synergistic intervention with Mg^{2+} and magnetic fields might exert osteogenic effects via the MAGT1 channel and CREB1 protein. This study provides an experimental basis for a potential Mg^{2+}-SMF synergistic artificial bone material that could be clinically applied in the treatment of bone defects.

1. Introduction

Magnesium ion (Mg^{2+})-based materials are expected to be applied in clinical practice, as they exert osteogenic effects and their mechanical properties are similar to those of the natural bone. Unfortunately, the rate of degradation of pure Mg-based materials that are used in orthopedics is extremely high. In the bone tissue, wherein fluid circulation and metabolism are relatively slow, this degradation can cause excessive local Mg^{2+} and hydrogen accumulation, resulting in a highly alkaline environment, which adversely affects the blood supply to surrounding soft tissues as well as cell adhesion and the repair of bone defects.

Biodegradable orthopedic materials have been extensively studied in recent years [1, 2], and numerous studies have shown that Mg^{2+} can promote the proliferation and osteogenic differentiation of bone marrow mesenchymal stem cells (BMSCs) [3–6]. In addition to promoting the differentiation of BMSCs into osteoblasts, Mg^{2+} can increase extracellular matrix (ECM) mineralization, resulting in excellent osteoinduction [7–9]. A previous study has confirmed that BMSCs display the best proliferation and

osteogenic differentiation when cultured with 7.5 mM Mg^{2+} [10]. In particular, Mg^{2+} can promote osteogenic differentiation by inducing cAMP responsive element binding protein 1 (CREB1) phosphorylation via the Mg^{2+} channel magnesium transporter 1 (MAGT1) [9]. Mg^{2+} can also induce BMSC differentiation into osteoblasts directly, via MAGT1, and promote the expression of intracellular osteogenic signaling molecules [alkaline phosphatase (ALP), OCN, COL1, and RUNX2]. Since osteogenic properties of Mg^{2+} are associated with its transmembrane transport, it is important to determine the mechanisms underlying the opening of the MAGT1 channel to induce Mg^{2+} influx. Therefore, an understanding of how to effectively open the MAGT1 channel in the cell membrane and cause an effective influx of Mg^{2+} is the key to achieving the full osteoinductive activity of Mg^{2+}.

The magnetic field environment can change the opening frequency of Mg^{2+} channel proteins on the cell membrane surface. Thus, the influx efficiency of Mg^{2+} can be improved to enhance its biological effect on osteogenesis. Numerous studies have shown that BMSC proliferation and osteoinduction can be accelerated by medium-strength magnetic fields (1 mT–1 T) [11–14], which include both pulsed electromagnetic fields (PEMFs) [15–17] and static magnetic fields (SMFs) [18–22]. Since magnetic fields are noninvasive and safe, they have the potential for broad clinical applications [23–27]. Although PEMFs are currently extensively studied for the induction of bone formation, SMFs have unique advantages for the preparation of artificial bone materials. For example, SMFs do not require powerful equipment for the biophysical stimulation of BMSCs, and it is easier to produce osteogenic effects when magnetic materials are added to artificial bone materials. SMFs can also exert important regulatory effects during bone metabolism and remodeling and have become an important biophysical tool for treating nonunions and promoting bone healing [28–30]. Studies have shown that SMFs can promote bone repair, bone deposition, and bone formation *in vitro* and *in vivo* [31–34]. In addition, SMFs can inhibit the reduction of the bone density caused by surgery or prostheses. Magnetic fields mainly exert osteogenic effects on BMSCs via electrical and mechanical receptors on the cell membrane that convert bioelectrical signals into biochemical signals, thereby activating intracellular signaling cascades. Indeed, osteogenesis-related ion channels, such as MAGT1, TWIK-related K^+ channel 1, and ORAI calcium release-activated calcium modulator 1/2, have been shown to alter their opening frequencies under the action of magnetic fields, thereby promoting osteogenesis [35–37]. However, it remains unclear whether the bioelectrical effects of a magnetic field could be combined with Mg^{2+} to regulate the osteogenic properties of ion channels and thereby synergistically enhance osteogenic differentiation and ECM mineralization.

In this study, we aimed to combine two factors with recognized osteogenic effects, Mg^{2+} and SMFs, in order to explore whether they can synergistically enhance bone formation while eliminating the disadvantages of Mg^{2+} as a potential new biomaterial. The findings of this study provide an experimental basis for a putative new type of Mg^{2+}-SMF synergistic artificial bone material with excellent osteogenic properties.

2. Materials and Methods

2.1. Cell Culture. BMSCs were purchased from Cyagen, Inc. (Beijing, China) and were grown in a BMSC growth medium at 37°C with 5% CO_2. The cells were cultured in Dulbecco's modified Eagle's medium (DMEM) containing 10% fetal bovine serum (FBS) and 1% penicillin and streptomycin in T25 culture flasks for expansion. To induce osteogenic differentiation, BMSCs were cultured in DMEM with 50 mM ascorbic acid, 10 mM dexamethasone, and 10 mM β-glycerophosphate (Sigma–Aldrich, St. Louis, MO, USA) at 37°C with 5% CO_2. The cells were divided into the following four groups: control (0 mM Mg^{2+} and 0 mT SMF), Mg^{2+} (7.5 mM Mg^{2+}), SMF (15 mT SMF), and Mg^{2+}-SMF (7.5 mM Mg^{2+} combined with 15 mT SMF) (Figure 1(a)), and their proliferation and osteogenic differentiation were observed. Mg^{2+} environment was added to the osteogenic induction medium in an appropriate proportion by anhydrous magnesium sulfate powder (aladdin⊠Shanghai, China), and sterilized by filtration with a 0.22 μm/28 mm filter (Beyotime, Shanghai, China).

2.2. Gene Silencing. Two genes (Magt1 and Creb1) were selected for silencing to verify their roles in the synergistic osteogenic effect of Mg^{2+} and the SMF. The same gene silencing method was used for both genes. BMSCs were cultured in 24-well plates for 36 h to reach 30–50% confluence. Transfection was performed with target gene-specific small interfering RNAs (siRNAs) using a siRNA transfection kit (RIBOBIO, Guangdong, China). The grouping included a nonspecific control (nc), siRNA (si), Mg^{2+}-SMF plus nonspecific control (ms + nc), and Mg^{2+}-SMF plus siRNA (ms + si), as shown in Figure 1(b). After transfection, the cell plate was incubated at 37°C with 5% CO2 for 48 h. The efficiency of siRNA transfection was observed under a fluorescence microscope (Leica, Wetzlar, Germany); a 30–50% proportion of fluorescently labeled cells indicated good transfection and successful silencing of the target gene. The cells were then cultured in different intervention environments for different times, and the expression levels of the osteogenic genes were evaluated in each group.

2.3. SMF Exposure. An SMF exposure system was produced using a neodymium (Nd2Fe14B) disc magnet (2 mm thick, 35 mm in diameter; Xinhongchang Magnets, Guangdong, China) and a 6-well culture plate (Figure 2). Briefly, the magnetic disc was placed above a well to expose the culture to a north magnetic field, and its strength was altered by controlling the distance between the magnetic disc and the culture plate. To stimulate BMSC osteogenesis, we used the optimal magnetic field strength of 15 mT, as has been shown in a previous study [13]. A Gauss meter (TS200; Sanliang, Tokyo, Japan) was used to measure the SMF strength.

2.4. Cell Proliferation Assay. To measure cell proliferation, we used a Cell Counting Kit-8 (CCK-8; Dojindo, Kumamoto, Japan). Briefly, BMSCs were seeded into 96-well plates

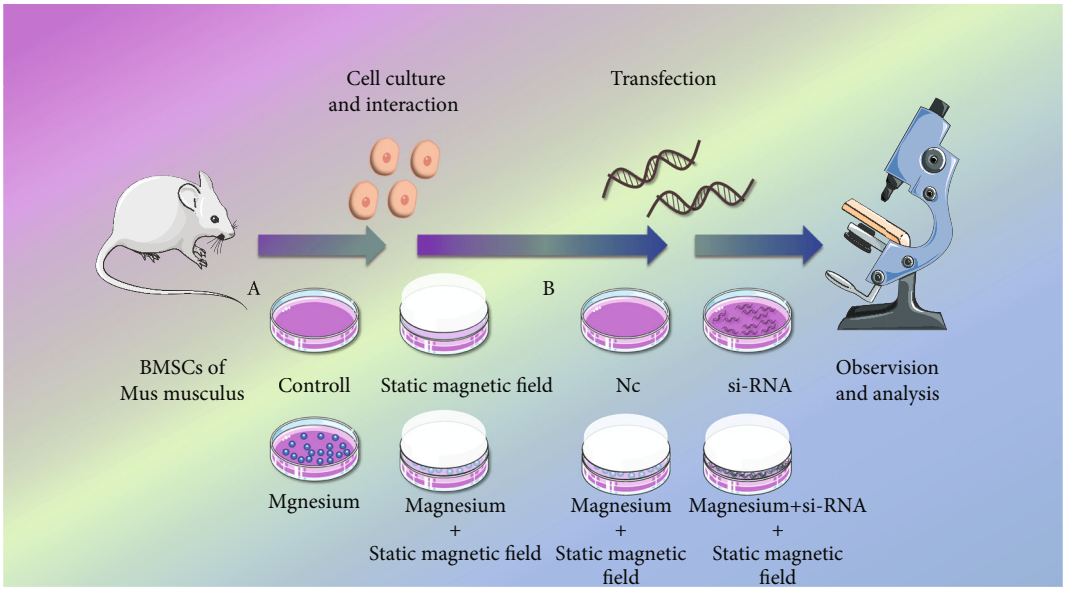

Figure 1: Study design. (a) BMSCs were divided into four groups: control, Mg^{2+}, SMF, and Mg^{2+}-SMF. This grouping was done to compare the differences between the magnetic field intervention alone, the magnesium ion intervention and the synergistic intervention. (b) SiRNA transfection was used to silence genes in the following groups: non-specific control (nc), siRNA (si), Mg^{2+}-SMF non-specific control (ms + nc), and Mg^{2+}-SMF siRNA (ms + si). nc and si to verify whether siRNA reagents are toxic to cells, ms + nc and ms + si to verify the role of target genes in synergistic osteogenesis.

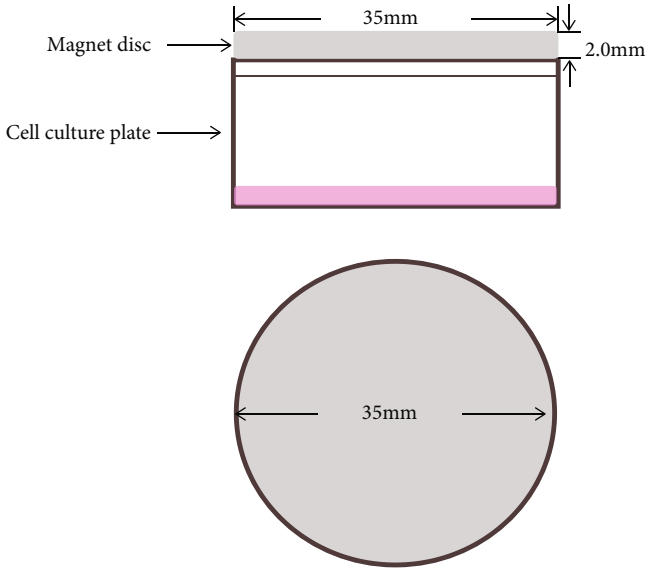

Figure 2: Schematic overview of SMF exposure system. A magnetic disc was placed above the wells of a 6-well culture plate to expose the culture to SMF.

(2×10^3 cells/well) and cultured at 37°C with 5% CO_2 for 1, 3, 5, or 7 days, with or without SMF exposure, in a medium with or without 7.5 mM Mg^{2+}. Cells that were cultured without SMF or Mg^{2+} exposure were used as a negative control. After incubation of plates with the CCK-8 reagents for 2 h, the absorbance was measured at 450 nm using a microplate reader (Bio-Rad, Hercules, CA, USA).

2.5. ALP Staining. BMSCs were seeded into a 6-well plate and cultured for 2 days to reach confluence. The cells were then cultured in an osteogenic medium containing DMEM supplemented with 10% FBS (Invitrogen. Waltham, MA, USA) and 50 μg/mL L-ascorbic acid (Sigma–Aldrich) at 37°C with 5% CO_2 for 7 days, with or without the SMF and/or Mg^{2+}, and the osteogenic medium was changed every 2 days. ALP staining was performed using a 5-bromo-4-chloro-3-indolylphosphate/nitro blue tetrazolium ALP color development kit (Beyotime, Shanghai, China) according to the manufacturer's instructions, and the cells were then observed under an optical microscope.

2.6. Alizarin Red Staining. Osteoblast differentiation was measured by quantifying the formation of mineralized bone nodules using an Alizarin Red staining assay. Briefly, BMSCs were seeded into a 6-well plate (4×10^4 cells/well) and cultured for 2 days to reach confluence. The cells were then cultured in the osteogenic medium at 37 ± 8°C with 5% CO_2 for 30 days, with or without the SMF and/or Mg^{2+}, then washed with phosphate-buffered saline, and stained with a 40 mM Alizarin Red solution for 10 min. After the cells were washed five times and decolorized with 10 mM sodium phosphate containing 10% cetylpyridinium chloride for 15 min at 26°C, Alizarin Red staining was quantified by Image J (National Institutes of Health, Bethesda, MD, USA).

2.7. Western Blot Analysis. ALP, RUNX2, OSX, and COL1 protein expression was measured using western blotting. Total protein was extracted from cells using radioimmunoprecipitation assay lysis buffer supplemented with 1% phenylmethanesulfonyl fluoride. Protein concentrations were measured using a Pierce bicinchoninic acid protein assay kit (Thermo Fisher Scientific, Waltham, MA, USA). Equal amounts of protein were separated by sodium dodecyl

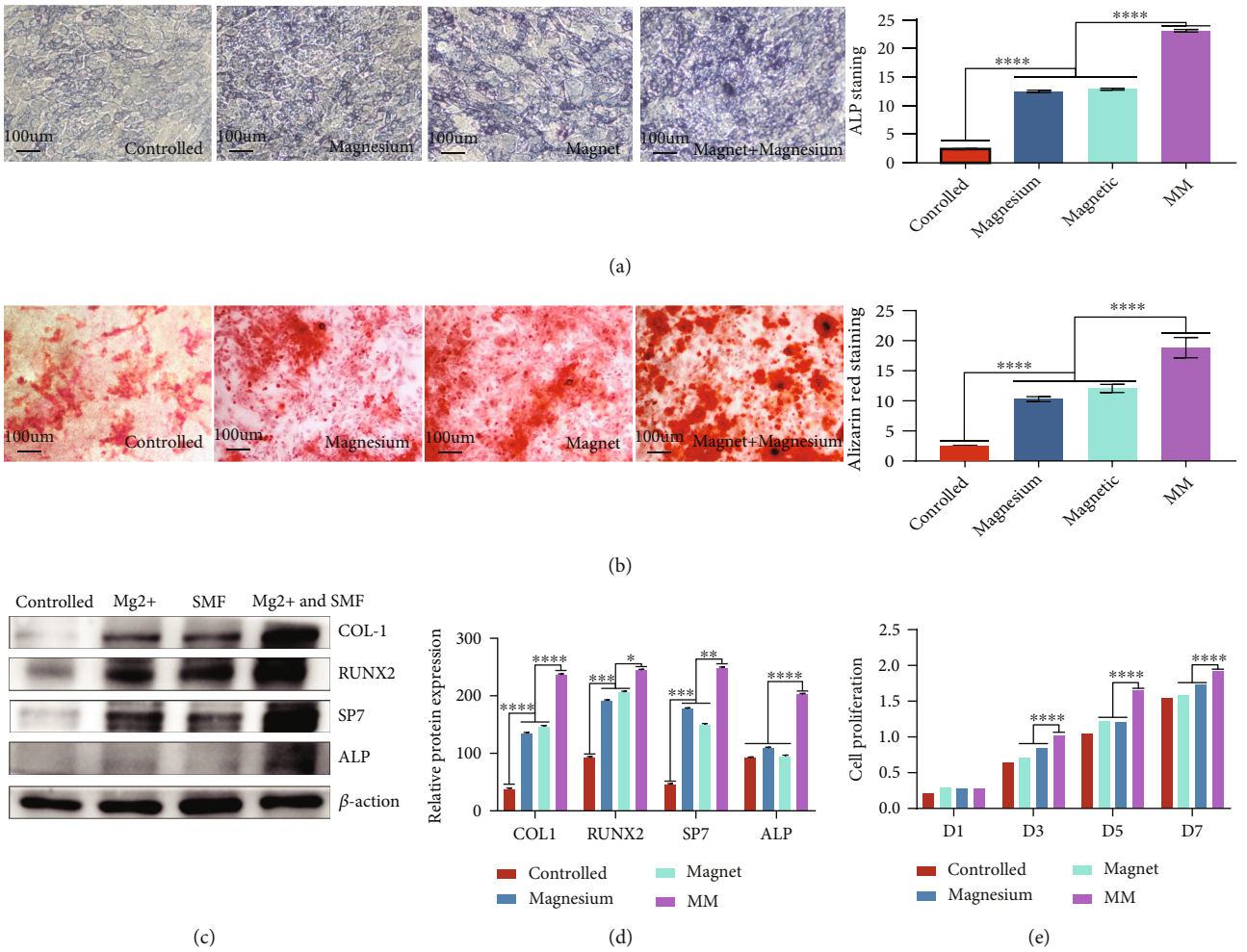

FIGURE 3: Osteogenic effects of Mg^{2+} and SMF. (a) Alp staining in BMSCs cultured for 7 days. Mg^{2+}-SMF synergy promoted BMSCs ALP activity. (b) Alizarin red staining to detect matrix mineralization in BMSCs cultured for 28 days. The most calcium nodules were observed in BMSCs treated with Mg^{2+}-SMF synergy. (c) Western blot analysis of protein expression in BMSCs cultured for 7 days. Mg^{2+} and SMF synergistically promoted the expression of BMSCs COL1, Runx2, SP7, and ALP. (d) Cell proliferation was assessed using CCK assays in BMSCs cultured for 1, 3, 5, and 7 days. Mg^{2+}-SMF synergy promoted BMSCs proliferation.

sulfate–polyacrylamide gel electrophoresis (10%) and transferred onto polyvinylidene fluoride membranes, which were then blocked with skim milk for 1 h and incubated with the following antibodies (Abcam, Shanghai, China) overnight at 4°C: anti-ALP (ab83259), anti-RUNX2 (ab23981), anti-Sp7/OSX (ab209484), and anti-collagen I (ab34710). The membranes were then washed three times with Tris-buffered saline containing 1‰ Tween 20 and incubated with IgG (heavy + light chains; ab205718) for 1 h. Protein bands were visualized using enhanced chemiluminescence detection (the protein bands were photographed after incubation with a chromogenic solution). Relative protein levels were determined by normalizing their expression to that of β-actin (ab119716).

2.8. Statistical Analysis. All experiments were conducted at least three times. Data were processed using the GraphPad Prism 9 software (GraphPad Software, San Diego, CA, USA) and expressed as the mean ± standard deviation. Differences between two groups were determined using the Student's *t*-test, and one-way analysis of variance with Tukey's multiple comparison test was used for multiple-group comparison. *P*-values of <0.05 were considered statistically significant.

3. Results

3.1. Effects of Mg^{2+} and the SMF on Differentiation and Proliferation of BMSCs. ALP staining showed (Figure 3(a)) that osteogenic differentiation was significantly enhanced in BMSCs treated with both Mg^{2+} and the SMF compared with that in BMSCs treated with either Mg^{2+} or the SMF alone and in the control group. Thus, the combination of Mg^{2+} and the SMF showed a synergistic effect and strongly promoted cell osteogenesis.

To determine the effect of the combination of Mg^{2+} with the SMF on ECM mineralization, BMSCs were stained with Alizarin Red after 28 days in culture. Cells treated with Mg^{2+} and the SMF in combination had the highest number of calcium nodules, while there was little difference in the number

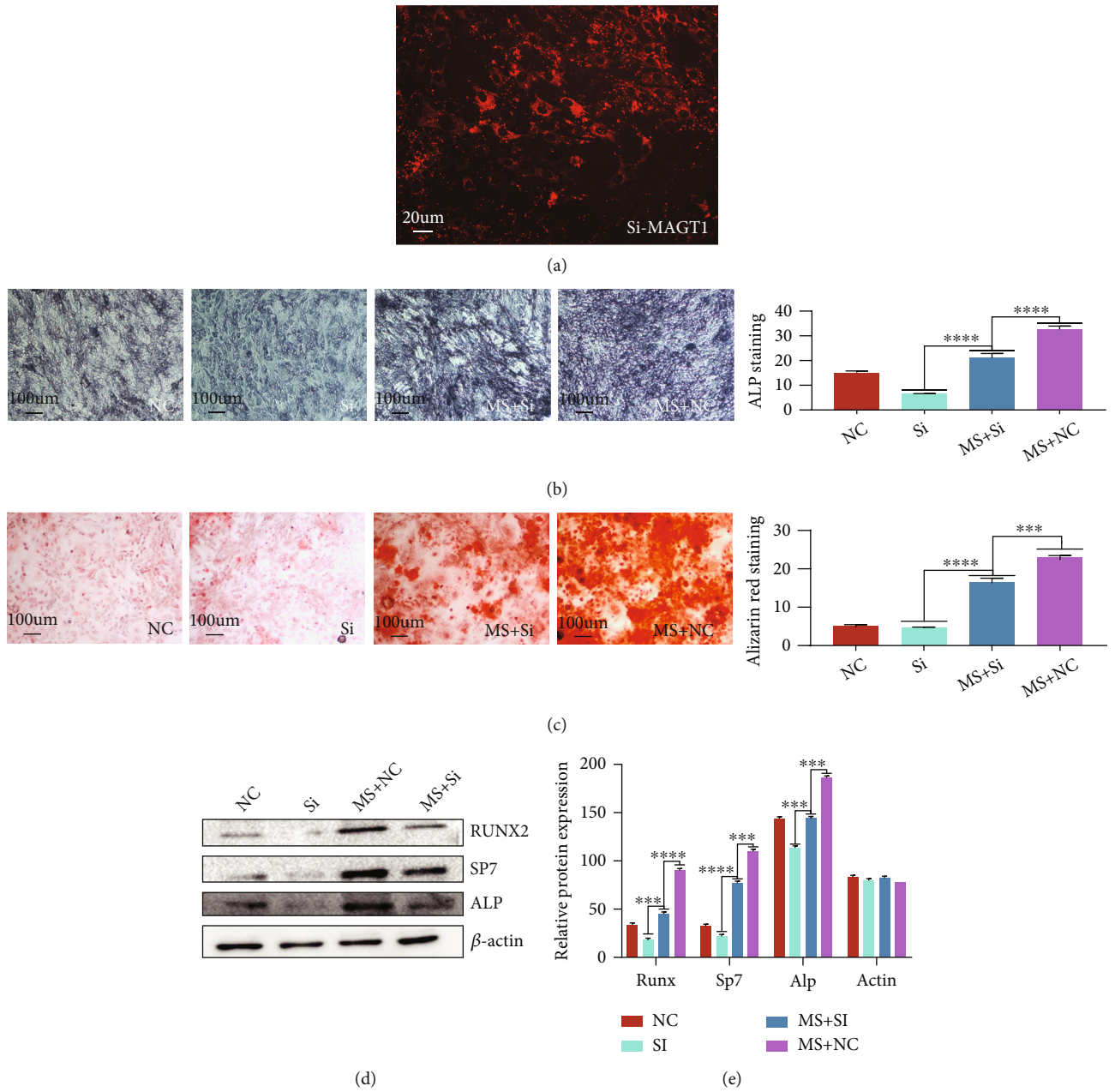

Figure 4: Effect of MAGT1 gene silencing on osteogenesis. (a) MAGT1 siRNA was transfected into BMSCs with an efficiency of 42%, indicating successful transfection. (b) MAGT1 siRNA interference decreased ALP staining after 7 days, indicating that Mg^{2+}-SMF induces osteogenesis via the MAGT1 gene. (c) MAGT1 siRNA interference decreased number of calcium nodules, suggesting that the MAGT1 gene plays a role in BMSCs osteogenesis and that Mg^{2+}-SMF induces osteogenesis via the MAGT1 gene. (d) MAGT1 siRNA interference decreased the protein expression of Runx2, SP7, and ALP in BMSCs.

of calcium nodules between BMSCs treated with Mg^{2+} or the SMF (Figure 3(b)). Thus, the combination of Mg^{2+} and the SMF showed the best performance in promoting ECM mineralization.

To confirm that Mg^{2+} and the SMF increased osteogenesis, protein expression of various osteogenic markers was measured. As shown in Figures 3(c) and 3(d), the combination of Mg^{2+} and the SMF increased the expression levels of the COL1, RUNX2, Sp7, and ALP proteins to a greater extent than either treatment alone. Thus, Mg^{2+} and the SMF synergistically increased the expression of representative osteogenic proteins in BMSCs.

To determine the effects of Mg^{2+} and the SMF on BMSC proliferation, cells were grown under different conditions, and their proliferation was measured on days 1, 3, 5, and 7. Cell proliferation did not significantly differ among the groups on day 1 (Figure 3(e)). However, the proliferation of BMSCs treated with Mg^{2+} or the SMF and, particularly, with both 7.5 mM Mg^{2+} and 15 mT SMF was higher than that in the control group on days 3 and 5. Moreover, on

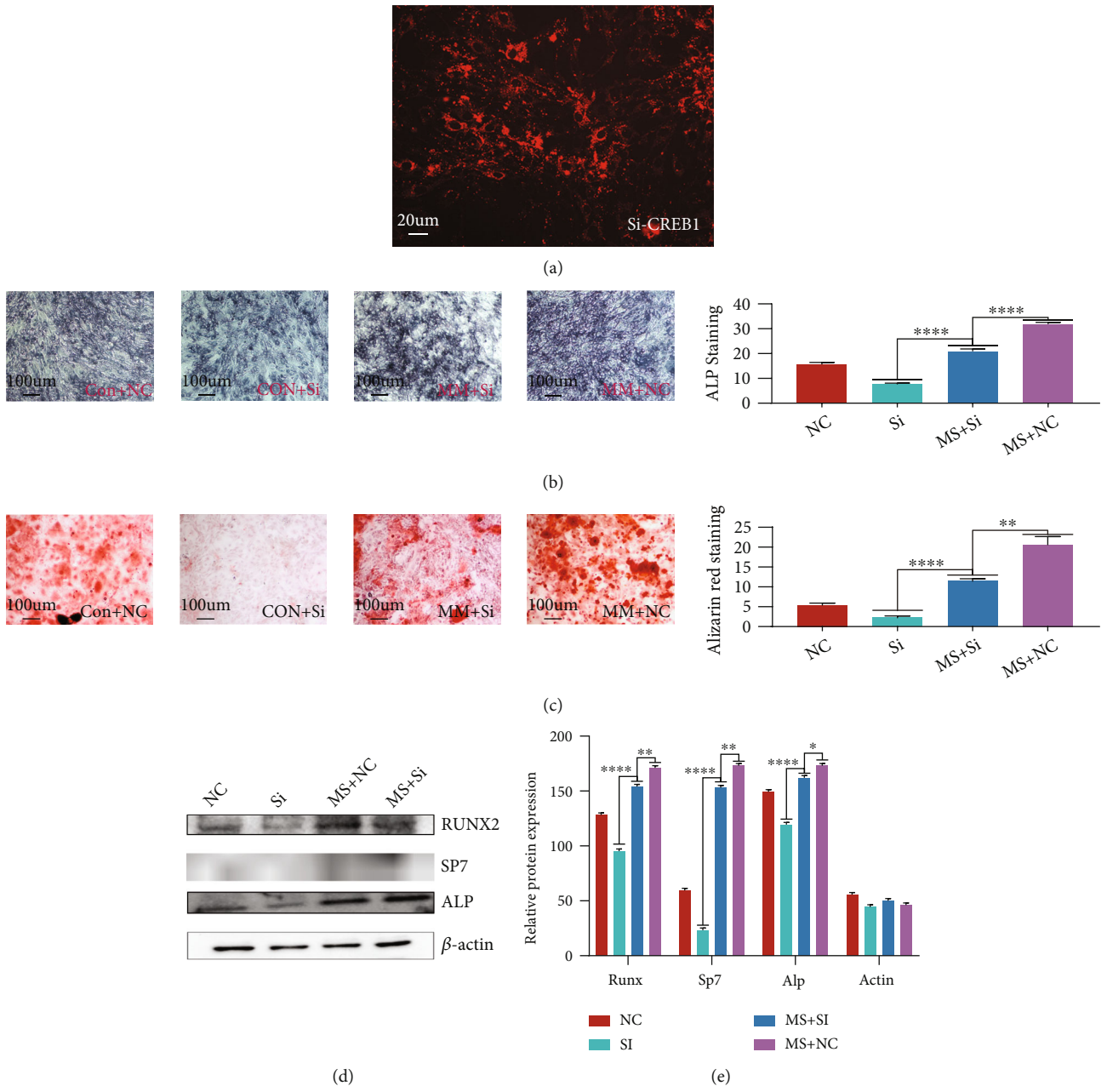

Figure 5: Effect of CREB1 gene silencing on osteogenesis. (a) CREB1 siRNA was transfected into BMSCs with an efficiency of 38%, indicating successful transfection. (b) CREB1 siRNA interference decreased Alp staining, indicating that Mg2 + -SMF induces osteogenesis via the CREB1 gene. (c) CREB1 siRNA interference decreased the number of calcium nodules, suggesting that the CREB1 gene plays a role in BMSCs osteogenesis. (d) CREB1 siRNA interference decreased the protein expression of Runx2, SP7, and ALP in BMSCs.

day 7, the proliferation was higher for BMSCs treated with both Mg^{2+} and the SMF than for those treated with Mg^{2+} and the SMF separately, and cell proliferation was higher in all three treatment groups than in the control group. Thus, the combination of Mg^{2+} and the SMF had the strongest proliferative effect on BMSCs. Taken together, these results showed that Mg^{2+} and the SMF synergistically enhanced the proliferation ability of BMSCs and their differentiation into osteoblasts compared with those in the groups treated with Mg^{2+} or SMF alone.

3.2. Effects of Magt1 and Creb1 Silencing on Osteogenesis. To investigate the roles of the MAGT1 channel and CREB1 protein in the synergistic osteogenic effects of Mg^{2+} and the SMF, both genes were silenced by transfecting BMSCs with the corresponding siRNAs. For *Magt1* silencing, the siRNA transfection efficiency was 42% (Figure 4(a)). ALP staining (Figure 4(b)), Alizarin Red staining (Figure 4(c)), and western blot analysis (Figures 4(d)–4(e)) revealed that the levels of osteogenic markers were lower in the siRNA group than in the nonspecific control siRNA group and in the Mg^{2+}-

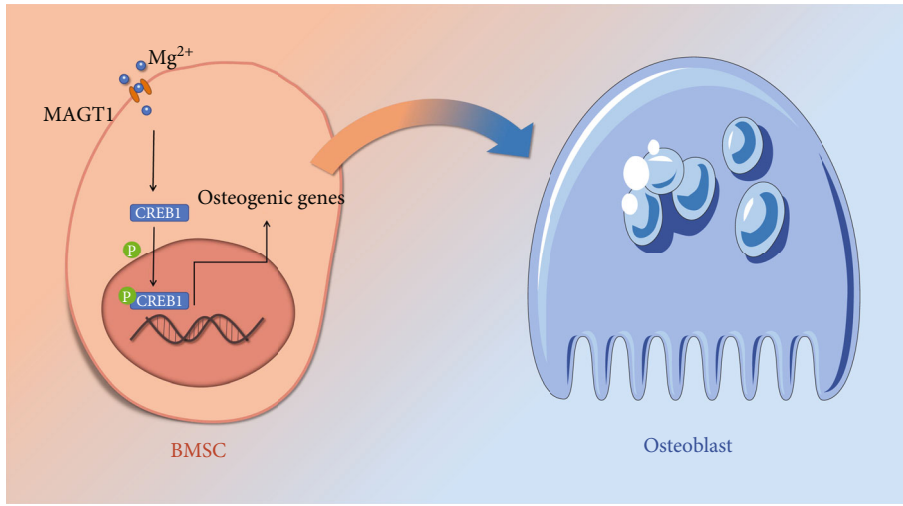

Figure 6: Osteogenic mechanism of Mg^{2+}. Mg^{2+} can activate CREB1 phosphorylation through the Mg^{2+} channel MAGT1 and promote osteogenic differentiation via transmembrane Mg^{2+} transport.

SMF-treated siRNA group than in the Mg^{2+}-SMF-treated nonspecific control siRNA group. Taken together, these findings suggested that Mg^{2+} and the SMF induced osteogenesis in BMSCs via the MAGT1 channel. The siRNA transfection efficiency was 38% (Figure 5(a)) in *Crreb1* silencing. Similar findings were obtained in ALP staining (Figure 5(b)), Alizarin Red staining (Figure 5(c)), and western blot analysis (Figures 5(d)–5(e)) when *Creb1* was silenced, indicating that the CREB1 protein also played a key role in the synergistic osteogenic mechanism of Mg^{2+}-SMF. These data indicated that the MAGT1 channel and CREB1 protein played important roles in the synergistic osteogenic effects of Mg^{2+} and the SMF.

4. Discussion

Mg^{2+}-based materials exert good osteogenic effects, and their mechanical properties are similar to those of the natural bone; however, these materials have not been applied clinically because of their high rate of degradation *in vivo*. Mg^{2+} can promote osteogenic differentiation by inducing CREB1 phosphorylation via the MAGT1 (Figure 6). According to this osteogenic property of Mg^{2+}, we need to find a means to promote the influx to improve the utilization efficiency of Mg^{2+}, so that only less Mg^{2+} is required to achieve a higher osteogenic effect. We found SMFs because it can change the opening frequency of Mg^{2+} channels to promote magnesium influx. Although SMFs can exert osteogenic effects via electrical and mechanical receptors on the cell membrane, it remains unclear whether the bioelectrical effects of a magnetic field could synergistically enhance osteogenic differentiation in combination with Mg^{2+}. Herein, we combined Mg^{2+} and an SMF to explore whether they can synergistically enhance bone formation while eliminating the disadvantages of Mg^{2+}-based biomaterials. Notably, we found that proliferation and osteogenic differentiation were significantly higher in BMSCs cotreated with Mg^{2+} and the SMF than in those treated with either intervention alone. Further gene silencing experiments suggested that these effects might be related to *Magt1* and *Creb1*. Collectively, our data demonstrated that Mg^{2+} and the SMF synergistically promoted the proliferation and osteogenic differentiation of BMSCs via the MAGT1 channel and CREB1 protein.

Several related studies have clearly demonstrated that certain Mg^{2+} concentrations and certain SMF intensities can promote BMSC proliferation and osteogenesis. Similarly, we observed that a synergistic intervention with Mg^{2+}-SMF significantly promoted the proliferation and induced osteogenic differentiation of BMSCs, which may be due to the effect of the SMF on MAGT1 channels on the cell membrane [38]. A previous study has shown that the opening frequency of ion channels on the cell membrane can change under the action of an SMF [39]. Therefore, SMFs can change the balance of the ion flow and membrane potential to promote bone formation and can also increase the opening frequency of MAGT1 channels to enhance the influx of Mg^{2+} to synergistically improve the osteogenic effect (Figure 7). Magnetic fields can modulate cellular functions, including cell morphology, cell cycle distribution, differentiation, proliferation, and gene expression [40]. This modulation may be due to electrodynamic interactions (Hall effect), magnetomechanical interactions, and radical pair effects [36]. Several studies have reported that different magnetic field environments have different effects on the cell differentiation ability. In particular, the effect of the magnetic field strength on cells has been a focus of research. As reported, S. Yamaguchi-Sekino, T. Kira, M. Sekino et al. found that the differentiation ability of cells was inhibited under the high-intensity magnetic field environment of 7 T [41]. They consider that SMFs may interfere with the opening of ion channels and hinder BMSC osteogenesis. However we found that a medium-strength (15 mT) SMF promoted cell proliferation and osteogenesis. These differences are likely to be caused by two-way differences in the magnetic field strength in a cellular environment. At present, it is believed that the high-intensity magnetic field environment has an inhibitory effect on the differentiation ability of cells, whereas a medium-intensity magnetic field has a more

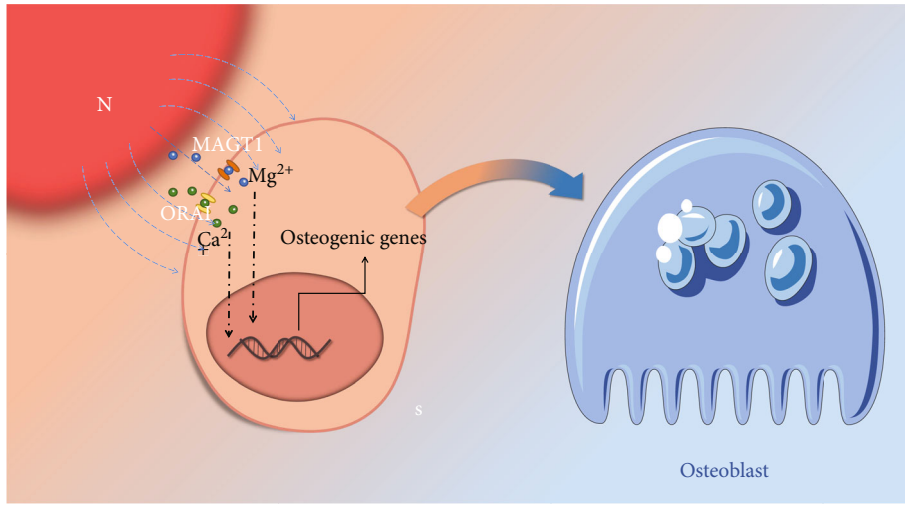

Figure 7: Mechanism of Mg2 + -SMF synergistic bone formation. Mg2 + -SMF increase the opening frequency of the MAGT1 channel, enhancing the influx of Mg2+ and thus the differentiation of BMSCs into osteoblasts.

beneficial biological effect. Our results confirmed that the medium-strength magnetic field was consistent with other articles to promote the osteogenic differentiation of BMSCs. In our experiments, compared with the control group, the SMF group showed stronger osteogenic properties in the results of ALP staining, Alizarin Red Staining and Western Blot.

Like the strength of the magnetic field, different types of magnetic fields have different effects on cell differentiation. A constant SMF with moderate intensity can induce the differentiation of BMSCs into osteoblasts by promoting the expression of related proteins. The sinusoidal electromagnetic field has a certain induction effect on the osteogenic differentiation of BMSCs, and the sinusoidal electromagnetic field of 1.0-2.0 mT, 10-50 Hz has the greatest effect on the differentiation of bone marrow mesenchymal stem cells [42]. So we fixed the most suitable magnetic field strength environment for experiments.

Magnetic field position and orientation also have different effects on cell differentiation. As reported by Lin, S. Y, Li, J et al., upon intervention of BMSCs in parallel and perpendicular magnetic field directions, the cells produced different differentiation states [43]. This may be due to the different angles of the magnetic poles and magnetic field lines to the cell. So we fixed the magnetic poles (using north magnetic poles for all interventions) to eliminate experimental errors.

To the best of our knowledge, this study is the first to demonstrate a synergistic effect between Mg^{2+} and the SMF in promoting BMSC proliferation and osteogenesis; however, the study has a few limitations. First, all experiments were performed using mouse BMSCs; therefore, further studies should examine the effects of Mg^{2+} and the SMF on BMSCs from other species, such as rabbits and humans. Similarly, since we only studied BMSCs cultured for 7 days, future experiments should extend the culture period and observe changes in osteogenic markers at different times. Finally, our research was based on the observations at the cellular level and thus may not reflect the process of bone formation in an organism. Subsequent studies are required to address these issues.

5. Conclusions

This study demonstrated that a medium-strength SMF intervention, combined with an appropriate Mg^{2+} concentration, could increase the expression of the COL1, Sp7, RUNX2, and ALP proteins in BMSCs via MAGT1 and CREB1 and significantly enhance the proliferation and osteoblast differentiation of BMSCs. Thus, Mg^{2+} and the SMF could be combined to develop new artificial bone materials with improved osteogenic properties to enhance bone cell proliferation and differentiation and promote the healing of bone defects. Future studies should identify the specific pathways through which Mg^{2+} and the SMF affect bone formation.

Abbreviations

MAGT1: Magnesium transporter 1
SMF: Static magnetic field
BMSCs: Bone mesenchymal stem cells
CCK-8 kit: Cell counting Kit-8
ALP: Alkaline phosphatase
CREB1: cAMP responsive element binding protein 1
PEMF: Pulsed electromagnetic fields
TREK1: TWIK-related K^+ channel 1
ORAI1/2: ORAI calcium release-activated calcium Modulator1/2.

Data Availability

The data used to support the findings of this study are included within the article.

Conflicts of Interest

The authors declare that they have no conflicts of interest.

Authors' Contributions

Youwen Deng and Cijun Shuai designed this work. Yifan Wang and Xin Wu integrated and analyzed the data. Yifan Wang, Xin Wu and Pei Feng wrote this manuscript. Pei Feng and Wei Tan edited and revised the manuscript. All authors approved this manuscript.

Funding

This work was supported by The Natural Science Foundation of China (81472058, 52105352); Hunan Science and Technology Innovation Plan (2018SK2105, 422000008); Science and Technology Program of Huizhou (No.2020Y253); Medical Science and Technology Research Fund Project of Guangdong Province (B2021166); Postgraduate Research and Innovation Project of Central South University (1053320210754).

Acknowledgments

The authors thank the members in Hunan Engineering Laboratory for Orthopedic Biomaterials and the department of spine surgery of the Third Xiangya Hospital of the Central South University.

Supplementary Materials

Supplementary 1. rawdata-ALP: Alkaline phosphatase (ALP) staining by 5-bromo-4-chloro-3-indolyl-phosphate/Nitro-Blue-Tetrazolium ALP color development kit.

Supplementary 2. rawdata-cck8: Cell proliferation assay by cell counting kit (cck8).

Supplementary 3. rawdata-red: Alizarin red staining, osteoblast differentiation was measured by quantifying the formation of mineralized bone nodules using an alizarin red staining assay.

Supplementary 4. rawdata-siRNA: Silence genes in BMSCs by transfecting the cells with corresponding siRNAs.

Supplementary 5. rawdata-wb: Western blot analysis. ALP, Runx2, Osx, and Col-I protein expression were measured using western blotting.

References

[1] Z. P. Du, X. X. Feng, G. X. Cao et al., "The effect of carbon nanotubes on osteogenic functions of adipose-derived mesenchymal stem cells in vitro and bone formation in vivo compared with that of nano-hydroxyapatite and the possible mechanism," *Bioactive Materials*, vol. 6, no. 2, pp. 333–345, 2021.

[2] L. Wang, C. Y. Wang, S. Wu, Y. B. Fan, and X. M. Li, "Influence of the mechanical properties of biomaterials on degradability, cell behaviors and signaling pathways: current progress and challenges," *Biomaterials Science*, vol. 8, no. 10, pp. 2714–2733, 2020.

[3] M. Bessa-Goncalves, A. M. Silva, J. P. Bras et al., "Fibrinogen and magnesium combination biomaterials modulate macrophage phenotype, NF-kB signaling and crosstalk with mesenchymal stem/stromal cells," *Acta Biomaterialia*, vol. 114, pp. 471–484, 2020.

[4] J. Nourisa, B. Zeller-Plumhoff, H. Helmholz, B. Luthringer-Feyerabend, V. Ivannikov, and R. Willumeit-Romer, "Magnesium ions regulate mesenchymal stem cells population and osteogenic differentiation: a fuzzy agent-based modeling approach," *Computational and Structural Biotechnology Journal*, vol. 19, pp. 4110–4122, 2021.

[5] J. W. Park, T. Hanawa, and J. H. Chung, "The relative effects of ca and mg ions on MSC osteogenesis in the surface modification of microrough Ti implants," *International Journal of Nanomedicine*, vol. 14, pp. 5697–5711, 2019.

[6] Q. Wang, L. Xu, R. Willumeit-Romer, and B. J. C. Luthringer-Feyerabend, "Macrophage-derived oncostatin M/bone morphogenetic protein 6 in response to mg-based materials influences pro-osteogenic activity of human umbilical cord perivascular cells," *Acta Biomaterialia*, vol. 133, pp. 268–279, 2021.

[7] Z. Zhai, X. Qu, H. Li et al., "The effect of metallic magnesium degradation products on osteoclast-induced osteolysis and attenuation of NF-kappaB and NFATc1 signaling," *Biomaterials*, vol. 35, no. 24, pp. 6299–6310, 2014.

[8] L. Zhang, C. Yang, J. Li, Y. Zhu, and X. Zhang, "High extracellular magnesium inhibits mineralized matrix deposition and modulates intracellular calcium signaling in human bone marrow-derived mesenchymal stem cells," *Biochemical and Biophysical Research Communications*, vol. 450, no. 4, pp. 1390–1395, 2014.

[9] Y. Zhang, J. Xu, Y. C. Ruan et al., "Implant-derived magnesium induces local neuronal production of CGRP to improve bone-fracture healing in rats," *Nature Medicine*, vol. 22, no. 10, pp. 1160–1169, 2016.

[10] W. Tang, Q. Liu, W. Tan, T. Sun, and Y. Deng, "LncRNA expression profile analysis of mg(2+)-induced osteogenesis by RNA-seq and bioinformatics," *Genes Genomics*, vol. 43, no. 11, pp. 1247–1257, 2021.

[11] C. Y. Chang, W. Z. Lew, S. W. Feng et al., "Static magnetic field-enhanced osteogenic differentiation of human umbilical cord-derived mesenchymal stem cells via matrix vesicle secretion," *International Journal of Radiation Biology*, vol. 96, no. 9, pp. 1207–1217, 2020.

[12] G. Chen, Y. Zhuo, B. Tao et al., "Moderate SMFs attenuate bone loss in mice by promoting directional osteogenic differentiation of BMSCs," *Stem Cell Research & Therapy*, vol. 11, no. 1, p. 487, 2020.

[13] F. Javani Jouni, P. Abdolmaleki, and M. Movahedin, "Investigation on the effect of static magnetic field up to 15 mT on the viability and proliferation rate of rat bone marrow stem cells," *In Vitro Cellular & Developmental Biology-Animal*, vol. 49, no. 3, pp. 212–219, 2013.

[14] L. Kong, Y. Han, Q. Lu et al., "Polydopamine coating with static magnetic field promotes the osteogenic differentiation of human bone-derived mesenchymal stem cells on three-dimensional printed porous titanium scaffolds by upregulation of the BMP-Smads signaling pathway," *American Journal of Translational Research*, vol. 12, no. 12, pp. 7812–7825, 2020.

[15] C. C. Lin, Y. T. Chang, R. W. Lin, C. W. Chang, G. J. Wang, and K. A. Lai, "Single pulsed electromagnetic field restores bone mass and microarchitecture in denervation/disuse osteopenic mice," *Medical Engineering & Physics*, vol. 80, pp. 52–59, 2020.

[16] F. Martini, A. Pellati, E. Mazzoni et al., "Bone Morphogenetic Protein-2 Signaling in the Osteogenic Differentiation of Human Bone Marrow Mesenchymal Stem Cells Induced by Pulsed Electromagnetic Fields," *International Journal of Molecular Sciences*, vol. 21, no. 6, 2020.

[17] Q. Ren, J. Zhou, M. G. Wang, and K. M. Chen, "Pulsed electromagnetic fields stimulating osteogenic differentiation and maturation involves primary cilia-PI3K/AKT pathway," *Beijing Da Xue Xue Bao. Yi Xue Ban*, vol. 51, no. 2, pp. 245–251, 2019.

[18] D. Wu, X. Chang, J. Tian et al., "Bone mesenchymal stem cells stimulation by magnetic nanoparticles and a static magnetic field: release of exosomal miR-1260a improves osteogenesis and angiogenesis," *Journal of nanobiotechnology*, vol. 19, no. 1, p. 209, 2021.

[19] Y. Naito, S. Yamada, Y. Jinno et al., "Bone-forming effect of a static magnetic field in rabbit femurs," *The International Journal of Periodontics & Restorative Dentistry*, vol. 39, no. 2, pp. 259–264, 2019.

[20] Y. He, G. Chen, Y. Li et al., "Effect of magnetic graphene oxide on cellular behaviors and osteogenesis under a moderate static magnetic field," *Nanomedicine*, vol. 37, article 102435, 2021.

[21] M. Filippi, B. Dasen, J. Guerrero et al., "Magnetic nanocomposite hydrogels and static magnetic field stimulate the osteoblastic and vasculogenic profile of adipose-derived cells," *Biomaterials*, vol. 223, article 119468, 2019.

[22] S. K. Boda, G. Thrivikraman, and B. Basu, "Magnetic field assisted stem cell differentiation - role of substrate magnetization in osteogenesis," *Journal of Materials Chemistry B*, vol. 3, no. 16, pp. 3150–3168, 2015.

[23] C. Androjna, C. S. Yee, C. R. White et al., "A comparison of alendronate to varying magnitude PEMF in mitigating bone loss and altering bone remodeling in skeletally mature osteoporotic rats," *Bone*, vol. 143, article 115761, 2021.

[24] J. Cai, W. Li, T. Sun, X. Li, E. Luo, and D. Jing, "Pulsed electromagnetic fields preserve bone architecture and mechanical properties and stimulate porous implant osseointegration by promoting bone anabolism in type 1 diabetic rabbits," *Osteoporosis International*, vol. 29, no. 5, pp. 1177–1191, 2018.

[25] M. M. Eid, A. M. El-Gendy, W. K. Abdelbasset, S. M. Elkholi, and M. S. Abdel-Fattah, "The effect of magnetic therapy and moderate aerobic exercise on osteoporotic patients: a randomized clinical study," *Medicine (Baltimore)*, vol. 100, no. 39, article e27379, 2021.

[26] G. Qian, M. Wang, Y. Dong, Y. Hong, Y. Yu, and J. Mei, "Effect of combined treatment with pulsed electromagnetic field stimulation and sclerostin monoclonal antibody on changes in bone metabolism and pedicle screw augmentation in rabbits with ovariectomy-induced osteoporosis," *Annals of Palliative Medicine*, vol. 10, no. 2, pp. 1070–1078, 2021.

[27] L. Wang, Y. Li, S. Xie, J. Huang, K. Song, and C. He, "Effects of pulsed electromagnetic field therapy at different frequencies on bone mass and microarchitecture in osteoporotic mice," *Bioelectromagnetics*, vol. 42, no. 6, pp. 441–454, 2021.

[28] W. Li, S. Zhao, W. He, M. Zhang, S. Li, and Y. Xu, "Static magnetic fields accelerate osteogenesis by regulating FLRT/BMP pathway," *Biochemical and Biophysical Research Communications*, vol. 527, no. 1, pp. 83–89, 2020.

[29] Z. Bao, M. Fan, L. Ma, Q. Duan, and W. Jiang, "The effects of pulsed electromagnetic fields combined with a static magnetic intramedullary implant on the repair of bone defects: a preliminary study," *Electromagnetic Biology and Medicine*, vol. 38, no. 3, pp. 210–217, 2019.

[30] K. Marycz, K. Kornicka, and M. Rocken, "Static magnetic field (SMF) as a regulator of stem cell fate-new perspectives in regenerative medicine arising from an underestimated tool," *Stem Cell Reviews and Reports*, vol. 14, no. 6, pp. 785–792, 2018.

[31] Z. Huang, Y. He, X. Chang et al., "A magnetic iron oxide/Polydopamine coating can improve osteogenesis of 3D-printed porous titanium scaffolds with a static magnetic field by upregulating the TGFbeta-Smads pathway," *Advanced Healthcare Materials*, vol. 9, no. 14, article e2000318, 2020.

[32] X. Li, Q. Zou, Y. Man, and W. Li, "Synergistic effects of novel superparamagnetic/Upconversion HA material and Ti/magnet implant on biological performance and long-term in vivo tracking," *Small*, vol. 15, no. 31, article e1901617, 2019.

[33] L. Hao, L. Li, P. Wang et al., "Synergistic osteogenesis promoted by magnetically actuated nano-mechanical stimuli," *Nanoscale*, vol. 11, no. 48, pp. 23423–23437, 2019.

[34] H. Zhang, L. Gan, X. Zhu et al., "Moderate-intensity 4mT static magnetic fields prevent bone architectural deterioration and strength reduction by stimulating bone formation in streptozotocin-treated diabetic rats," *Bone*, vol. 107, pp. 36–44, 2018.

[35] A. Russo, M. Bianchi, M. Sartori et al., "Magnetic forces and magnetized biomaterials provide dynamic flux information during bone regeneration," *Journal of Materials Science. Materials in Medicine*, vol. 27, no. 3, p. 51, 2016.

[36] J. Zhang, C. Ding, L. Ren, Y. Zhou, and P. Shang, "The effects of static magnetic fields on bone," *Progress in Biophysics and Molecular Biology*, vol. 114, no. 3, pp. 146–152, 2014.

[37] J. M. Kanczler, H. S. Sura, J. Magnay et al., "Controlled differentiation of human bone marrow stromal cells using magnetic nanoparticle technology," *Tissue Engineering. Part A*, vol. 16, no. 10, pp. 3241–3250, 2010.

[38] J. Zheng, X. Mao, J. Ling, C. Chen, and W. Zhang, "Role of magnesium transporter subtype 1 (MagT1) in the osteogenic differentiation of rat bone marrow stem cells," *Biological Trace Element Research*, vol. 171, no. 1, pp. 131–137, 2016.

[39] D. Mohanta, E. Stava, M. Yu, and R. H. Blick, "Creation and regulation of ion channels across reconstituted phospholipid bilayers generated by streptavidin-linked magnetite nanoparticles," *Physical Review. E, Statistical, Nonlinear, and Soft Matter Physics*, vol. 89, no. 1, article 012707, 2014.

[40] J. Miyakoshi, "Effects of static magnetic fields at the cellular level," *Progress in Biophysics and Molecular Biology*, vol. 87, no. (2-3), pp. 213–223, 2005.

[41] S. Yamaguchi-Sekino, T. Kira, M. Sekino, and M. Akahane, "Effects of 7 T static magnetic fields on the expression of biological markers and the formation of bone in rats," *Bioelectromagnetics*, vol. 40, no. 1, pp. 16–26, 2019.

[42] F. Luo, T. Y. Hou, Z. H. Zhang, Z. Xie, X. H. Wu, and J. Z. Xu, "Effects of pulsed electromagnetic field frequencies on the osteogenic differentiation of human mesenchymal stem cells," *Orthopedics*, vol. 35, no. 4, pp. E526–E531, 2012.

[43] S. Y. Lin, J. Li, J. Q. Shao et al., "Anisotropic magneto-mechanical stimulation on collagen coatings to accelerate osteogenesis," *Colloids and Surfaces B-Biointerfaces*, vol. 210, p. 112227, 2022.